

DIPLOMARBEIT

Untersuchungen des Hochtemperaturkorrosionsverhaltens von P9 Stahl und Alloy 800HT in HCl- und H₂S- Atmosphären bei niedrigem Sauerstoffdruck

Ausgeführt zum Zweck der Erlangung des akademischen Grades einer
Diplom-Ingenieurin (Dipl.-Ing. oder DI)

eingereicht an der TU Wien
Fakultät für Maschinenwesen und Betriebswissenschaften
von

Magdalena ENGELMANN
(01125597)

Weigelsdorf 25
4115 Kleinzell im Mühlkreis

Unter der Leitung von
Ao.Univ.Prof. Dipl.-Chem. Dr. rer.nat Matthias Weil
Institut für Chemische Technologien und Analytik

Datum

Unterschrift (Studentin)

MASTER THESIS

Investigation of High-temperature Corrosion Behaviour of P9 steel and Alloy 800HT in HCl and H₂S Atmospheres with Low Oxygen Pressure

Carried out for the purpose of the degree of Master of Science
(MSc or Dipl.-Ing. or DI)

Submitted at TU Wien
Faculty of Mechanical and Industrial Engineering
by

Magdalena ENGELMANN
(01125597)

Weigelsdorf 25
4115 Kleinzell im Mühlkreis

Under the supervision of
Ao.Univ.Prof. Dipl.-Chem. Dr. rer.nat Matthias Weil
Department for Chemical Technologies and Analytics

Danksagung

Meinen Betreuern Herrn *Ao.Univ.Prof. Dipl.-Chem. Dr. rer.nat Matthias Weil* und *Dipl.-Ing Alexander Schmid* möchte ich für die hervorragende Betreuung und Unterstützung während meiner Zeit als Diplomandin danken, insbesondere dem *Alexander*, der Teile der Probenpräparation und REM / EDX Analysen an der Montanuniversität Leoben durchführte.

Für die finanzielle Unterstützung zur Durchführung dieser Arbeit bedanke ich mich bei der Firma OMV.

Zu danken habe ich natürlich auch (und nicht zuletzt) meinem Freund *Valentin*, meinen Studienkollegen und Freunden, die mich vor allem an nicht ganz so sonnigen Tagen wieder motivierten.

Mein ganz besonderer Dank gilt meinen Eltern *Marianne und Anton* und meinen Geschwistern *Katharina und Bernhard*, die mich während der Erstellung dieser Arbeit aber auch während meines gesamten Studiums immer unterstützten.

Abstract

The corrosion behaviour of Alloy 800HT and P9 steel was investigated in atmospheres mimicking the thermal cracking process of anthropogenic resources. The testing gas consisted of 3.8 vol.% HCl, 2.8 vol.% H₂, 1.9 vol.% CO₂, 0.3 vol.% CO, 0.02 vol.% H₂S and N₂ as balance. Additionally, experiments without HCl as corrosive component were performed to get more information about the influence of HCl on the high-temperature corrosion of the samples in mixed-gas atmospheres. The tests were performed between 24, 72 and 240 hours at 480 °C, 580 °C and 680 °C, respectively.

All samples showed solid corrosion products on their surfaces. Selected specimens were cold mounted to analyse the microstructure of the corrosion layers. SEM (scanning electron microscopy) / EDX (energy-dispersive X-ray spectroscopy) were used as complementary analytical methods for investigation of the corrosion process. Additionally XRD (X-ray powder diffraction) analyses of single corrosion products were made. Mass loss determinations for every specimen were performed as well.

The P9 steel showed an increasing mass loss with rising temperature, whereas alloy 800HT was quite resistant against HCl attack; only at lower temperatures the sulfidation of nickel led to an increase of the mass loss. The corrosion layers on the samples typically consisted of sulfide crystals on the outer layer, followed by an oxide/chloride scale with material depletion beneath it.

Zusammenfassung

Das Korrosionsverhalten der zwei Werkstoffe Alloy 800HT und P9 Stahl wurde unter einer bestimmten Gasatmosphäre untersucht. Das Prüfgas bestand aus 3.8 vol.% HCl, 2.8 vol.% H₂, 1.9 vol.% CO₂, 0.3 vol.% CO, 0.02 vol.% H₂S mit N₂ als Trägergas. Diese Zusammensetzung sollte die Bedingungen in der Gasatmosphäre einer Thermischen Cracking Anlage für anthropogene Ressourcen nachstellen. Zusätzlich wurden Versuche ohne HCl durchgeführt, um den Einfluss des Chlorwasserstoffes bei der Hochtemperaturkorrosion in Mischgasen zu ermitteln. Die Versuche wurden bei den drei unterschiedlichen Temperaturen 480 °C, 580 °C und 680 °C durchgeführt. Außerdem gab es drei Testzeiten von 24, 72 und 240 Stunden, um Informationen bezüglich der Zeitabhängigkeit des Korrosionsmechanismus zu erhalten.

Nach den Experimenten waren alle Proben mit einer Schicht fester Korrosionsrückstände umgeben. Um die Mikrostruktur dieser Korrosionsschichten zu ermitteln, wurden REM (Rasterelektronenmikroskopie) / EDX (energiedispersive Röntgenspektroskopie) Analysen durchgeführt. Als zusätzliche Analysemethode für einzelne Korrosionsrückstände wurden XRD (Röntgendiffraktometrie) Messungen durchgeführt. Weiteres wurde der Masseverlust pro Oberfläche für alle Proben berechnet.

Die zwei Werkstoffe zeigten unterschiedliche Ergebnisse des Korrosionsverhaltens. Der niedrig legierte P9 Stahl zeigte einen steigenden Masseverlust bei Erhöhung der Temperatur. Der Werkstoff Alloy 800HT, welcher auch als sehr korrosionsbeständig eingestuft wird, hatte einen vergleichsweise geringen Masseverlust, mit Ausnahme der niedrigsten Temperatur. Hier kam es aufgrund von Sulfidierung des Nickels zu einer leichten Erhöhung des Masseverlustes.

Typischerweise bestand die Korrosionsschicht aus äußeren Sulfidkristallen, gefolgt von einer porösen Oxid-/Chlorid-Zunderschicht und einer darunterliegenden Materialverarmung.

Table of contents

1	Introduction.....	1
2	Basic information	2
2.1	Thermodynamics.....	2
2.2	Corrosion kinetics in gases.....	3
2.3	Corrosion	6
2.4	High-temperature corrosion.....	7
2.5	High-temperature chlorine-induced corrosion.....	8
2.5.1	Corrosion in gaseous HCl without O ₂	9
2.5.2	Corrosion in gaseous HCl with O ₂	10
2.6	High-temperature sulfidation	13
2.7	High-temperature sulfidation and chlorination.....	15
3	Methods of analysis	16
3.1	SEM / EDX	16
3.2	XRD	16
4	Experimental procedure.....	18
5	Results and Discussion	23
5.1	Mass loss measurements.....	23
5.2	Corrosion products.....	26
5.2.1	Gas atmosphere with HCl	26
5.2.1.1	480 °C.....	27
5.2.1.2	580 °C.....	33
5.2.1.3	680 °C.....	38
5.2.2	Gas atmosphere without HCl.....	43
5.2.2.1	480 °C.....	43
5.2.2.2	680 °C.....	47
5.3	Microstructure analysis.....	51
5.3.1	Gas atmosphere with HCl	51
5.3.2	Gas atmosphere without HCl.....	52

5.4	Thermodynamic considerations.....	54
5.4.1	Gas atmosphere with HCl	54
5.4.1.1	480 °C.....	55
5.4.1.2	580 °C.....	56
5.4.1.3	680 °C.....	57
5.4.2	Gas atmosphere without HCl.....	58
5.5	Summary of the proposed corrosion mechanism.....	60
6	Conclusions.....	61
	References.....	62

Figures

Figure 2.1	Linear oxidation rate [11].....	4
Figure 2.2	Logarithmic and inverse logarithmic oxidation rate [11].....	5
Figure 2.3	Parabolic oxidation rate [12].....	5
Figure 2.4	Diffusion model for mass transport through metal oxide (MO) scale [15]...	6
Figure 2.5	Corrosion cell [17].....	7
Figure 2.6	Temperature dependence of equilibrium vapour pressures of solid metal chlorides [1].....	9
Figure 2.7	Schematic overview of the simultaneous growth and evaporation of the metal chlorides [12].....	10
Figure 2.8	Schematic overview of the 'active oxidation' for in a Cl ₂ containing atmosphere [26].....	11
Figure 2.9	Ellingham diagram for selected sulfides [28].....	14
Figure 4.1	Scheme of the testing equipment.....	18
Figure 4.2	Experimental setup.....	19
Figure 4.3	Real furnace temperatures.....	19
Figure 4.4	Silica glass holder without and with samples.....	21
Figure 4.5	Mass loss of a non-corroded P9 steel sample in 5% HCl after several measurements of 30 sec each.....	21
Figure 5.1	Mass loss of the alloys after 24 h at different temperatures.....	24
Figure 5.2	Mass loss of the alloys after 72 h at different temperatures.....	24
Figure 5.3	Mass loss of the alloys after 240 h at different temperatures.....	24
Figure 5.4	Iron(II) chloride in the colder part of the silica glass pipe.....	24
Figure 5.5	Mass loss of the alloys after 240 h in the 100:0 mixture at different temperatures.....	25
Figure 5.6	Comparison of the mass loss after 240 h in the 100:0 and 50:50 mixture and the mass loss of P9 after 72 h at 680 °C.....	25
Figure 5.7	Kinetic curves at 480 °C from alloy 800HT and P9 steel after 24, 72 and 240 h.....	26
Figure 5.8	Kinetic curves at 580 °C from alloy 800HT and P9 steel after 24, 72 and 240 h.....	26
Figure 5.9	Kinetic curves at 680 °C from alloy 800HT and P9 steel after 24, 72 and 240 h.....	26
Figure 5.10	Alloy 800HT after 240 h at 480 °C in the gas atmosphere with HCl.....	28
Figure 5.11	Alloy 800HT after 240 h at 480 °C in the gas atmosphere with HCl, after exposure to ambient atmosphere.....	28
Figure 5.12	P9 steel after 240 h at 480 °C in the gas atmosphere with HCl.....	28

Figure 5.13	Re-crystallized FeCl ₂ in the silica glass tube after 72 h at 480 °C.....	28
Figure 5.14	Cross section of alloy 800HT at 480 °C after 240 h in the 50:50 gas mixture.....	30
Figure 5.15	Cross section of the P9 steel at 480 °C after 240 h in the 50:50 gas mixture.....	30
Figure 5.16	EDX mapping of a cross section of alloy 800HT at 480 °C after 240 h in the 50:50 mixture. The colour is connected with the concentration and increases from dark blue, light blue, green, yellow, orange to red.....	31
Figure 5.17	EDX mapping of a cross section of P9 steel at 480 °C after 240 h in the 50:50 mixture. The colour is connected with the concentration and increases from dark blue, light blue, green, yellow, orange to red.....	32
Figure 5.18	Alloy 800HT after 240 h at 580 °C in the 50:50 gas atmosphere.....	33
Figure 5.19	P9 steel after 240 h at 580 °C in the 50:50 gas atmosphere.....	33
Figure 5.20	Re-crystallized FeCl ₂ in the silica glass pipe after 240 h at 580 °C.....	33
Figure 5.21	Cross section of alloy 800HT after 240 h at 580 °C.....	35
Figure 5.22	Cross section of P9 steel after 240 h at 580 °C.....	35
Figure 5.23	EDX mapping of a cross section of alloy 800HT at 580 °C after 240 h in the 50:50 mixture. The colour is connected with the concentration and increases from dark blue, light blue, green, yellow, orange to red.....	36
Figure 5.24	EDX mapping of a cross section of P9 steel at 580 °C after 240 h in the 50:50 mixture. The colour is connected with the concentration and increases from dark blue, light blue, green, yellow, orange to red.....	37
Figure 5.25	Alloy 800HT after 72 h at 680 °C in the 50:50 gas atmosphere.....	38
Figure 5.26	P9 steel after 72 h at 680 °C in the 50:50 gas atmosphere.....	38
Figure 5.27	P9 steel at 680 °C after 72 h in the 50:50 gas atmosphere, cleaned.....	38
Figure 5.28	Re-crystallized FeCl ₂ in the silica glass tube after 72 h at 680 °C.....	38
Figure 5.29	Cross section of alloy 800HT after 240 h at 680 °C.....	40
Figure 5.30	Cross section of P9 steel after 72 h at 680 °C.....	40
Figure 5.31	EDX mapping of a cross section of alloy 800HT at 680 °C after 240 h. The colour is connected with the concentration and increases from dark blue, light blue, green, yellow, orange to red.....	41
Figure 5.32	EDX mapping of a cross section of P9 steel at 680 °C after 72 h. The colour is connected with the concentration and increases from dark blue, light blue, green, yellow, orange to red.....	42
Figure 5.33	Alloy 800HT after 240 h at 480 °C in the 100:0 gas atmosphere.....	43
Figure 5.34	P9 steel after 240 h at 480 °C in the 100:0 gas atmosphere.....	43
Figure 5.35	Cross section of alloy 800HT after 240 h at 480 °C.....	44
Figure 5.36	Cross section of P9 steel after 240 h at 480 °C.....	44

Figure 5.37	EDX mapping of a cross section of alloy 800HT at 480 °C after 240 h in the 100:0 mixture. The colour is connected with the concentration and increases from dark blue, light blue, green, yellow, orange to red.....	45
Figure 5.38	EDX mapping of a cross section of P9 steel at 480 °C after 240 h in the 100:0 mixture. The colour is connected with the concentration and increases from dark blue, light blue, green, yellow, orange to red.....	46
Figure 5.39	Alloy 800HT after 240 h at 680 °C in the 100:0 gas atmosphere.....	47
Figure 5.40	P9 steel after 240 h at 680 °C in the 100:0 gas atmosphere.....	47
Figure 5.41	P9 steel after 240 h at 680 °C in the 100:0 gas atmosphere, cleaned.....	47
Figure 5.42	Cross section of alloy 800HT after 240 h at 680 °C in the 100:0 mixture...	48
Figure 5.43	Cross section of P9 steel after 240 h at 680 °C in the 100:0 mixture.....	48
Figure 5.44	EDX mapping of a cross section of alloy 800HT at 680 °C after 240 h in the 100:0 mixture. The colour is connected with the concentration and increases from dark blue, light blue, green, yellow, orange to red.....	49
Figure 5.45	EDX mapping of a cross section of P9 steel at 680 °C after 240 h in the 100:0 mixture. The colour is connected with the concentration and increases from dark blue, light blue, green, yellow, orange to red.....	50
Figure 5.46	Light microscopy pictures (magnification 200x) of the cleaned samples after the experiments in the 50:50 mixture: Alloy 800HT: (a) 480 °C; (b) 580 °C; (c) 680 °C // P9 steel (d) 480 °C; (e) 580 °C; (f) 680 °C.....	52
Figure 5.47	Light microscopy pictures (magnification 200x) of the cleaned samples after the experiments in the 50:50 mixture: Alloy 800HT etched with Beraha-II: (a) 480 °C; (b) 680 °C // P9 steel etched with Beraha-I: (c) 480 °C; (d) 680 °C.....	53
Figure 5.48	Schematic representation of the proposed corrosion mechanism in the mixed gas atmosphere: ① Initiation; ② Attack along grain boundaries and formation of metal chlorides (Me=Cr, Fe); ③ Reaction with H ₂ S and H ₂ O in the testing gas, formation of oxides and sulfides under release of HCl, re-entering of HCl; ④ Formation of large sulfide crystals on top of porous oxide layer with porous structure beneath it.....	60

Tables

Table 4.1	Chemical composition of the used iron alloys according to the manufacturer in wt.%.....	19
Table 4.2	Dimensions of the samples.....	19
Table 4.3	Composition of the test gases.....	20
Table 4.4	Required temperatures and periods of the experiments.....	20
Table 5.1	Etching periods for the samples in the gas atmosphere with HCl.....	51
Table 5.2	Etching periods for the samples in the gas atmosphere without HCl.....	53

1 Introduction

High-temperature corrosion of stainless steels is a problem in numerous industrial applications.[1, 2] In waste-to-energy plants, for example, high-temperature corrosion occurs due to the high chlorine concentration of the municipal solid waste, which is between 0.5-2.0wt.%. One of the main sources for this chlorine concentration in the municipal solid waste is sodium chloride.[3] Likewise, coals used as burning materials in power plants or coal gasification systems often contain chlorine as impurities. Therefore these applications suffer from the chlorine induced corrosion attack, too.[4]

The thermal cracking of long-chained hydrocarbons provided by agricultural, industrial or anthropogenic resources becomes more and more important. The thermal cracking process not only produces short-chained hydrocarbons needed for cheap synthetic crude oil, but also appears as a good recycling method. The feedstock for this thermal cracking often contains polyvinyl chloride (PVC). PVC is one of the most important polymers and reached a consumption of 38.5 million tons in 2013. Although PVC has a very long service life, it will eventually end up as solid waste. To avoid landfill, recycling is needed. However, PVC in the feedstock leads to the formation of corrosive HCl during the cracking process.[5]

The degradation of metallic materials due to high-temperature corrosion strongly depends on the surrounding environment. If the atmosphere contains corrosive components like HCl, most materials are unable to form a protective oxide scale and therefore suffer from severe mass loss above temperatures of 450 °C.[6] The reason for this mass loss is the formation of volatile metal chlorides with the consequence of creating a very porous and consequently non-protective oxide layer with a high tendency to spall.[7]

Anthropogenic resources used for the cracking process often do not only contain chlorine but also sulfur as an impurity, in particular in organic components like synthetic textiles.[8, 9] This leads to the formation of a gas atmosphere with additional H₂S. Only a few studies were devoted to the high-temperature corrosion in environments containing both HCl and H₂S gases. The results of these investigations led to conflicting conclusions. According to Pan et al. [2], addition of HCl in an oxidising-sulfidising atmosphere leads to an accelerated corrosion, whereas a decreasing corrosion rate by adding HCl to an oxidising-sulfidising environment was deduced by other authors.[10]

The main objective of the current master thesis is to find a suitable reactor material for the thermal cracking process of anthropogenic resources. Two different materials were tested: P9 steel and alloy 800HT. The P9 steel was chosen because of its low costs, whereas alloy 800HT is known as very resistant in environments with high-temperature corrosion. For comparison, all experiments were performed under constant temperatures, pressures and mass flow.

2 Basic information

2.1 Thermodynamics

The thermodynamics of a reaction gives information about the stability of the products. The driving force in every chemical reaction is the Gibbs energy change ΔG [J/mol]. It can be described with the Second Law of Thermodynamics:

$$\Delta G = \Delta H - T * \Delta S \quad (2.1)$$

ΔH Enthalpy of reaction [J/mol]

T Absolute temperature [K]

ΔS Entropy change [J/(mol*K)]

If the change of the Gibbs energy is negative, the reaction will run spontaneously. $\Delta G = 0$ means the reaction reached its equilibrium, and if the Gibbs energy change is positive, the reverse reaction will be favoured.

Another way to express ΔG is by using the standard Gibbs energy change ΔG^0 [J/mol]. It leads, for a reaction $aA + bB = cC + dD$, to:

$$\Delta G = \Delta G^0 + R * T * \ln \frac{a_C^c * a_D^d}{a_A^a * a_B^b} \quad (2.2)$$

a Chemical activity [-]

R Gas constant [J/(mol*K)]

The reaction of a general oxidation process of a metal is shown in equation 2.3.



Usually solid materials, like metals and their oxides, have an activity of 1, and in case of high-temperature corrosion with reasonable pressures, the activity of oxygen is approximately proportional to its partial pressure. Under these assumptions the standard Gibbs energy change can be expressed at the equilibrium of the reaction ($\Delta G = 0$) with:

$$\Delta G^0 = -R * T * \ln \left(\frac{1}{p_{O_2}} \right) = R * T * \ln(p_{O_2}) \rightarrow p_{O_2} = \exp \left(\frac{\Delta G^0}{R * T} \right) \quad (2.4)$$

Based on this equation and an Ellingham diagram it is possible to calculate the partial pressure needed for formation of the oxides and to find out whether the metal oxides are stable under certain conditions.[11, 12]

In case of sulfidation and the resulting formation of metal sulfides, not the oxide but the sulfide partial pressure is valid. In a mixed gas atmosphere containing H_2S and H_2 , the partial pressure of the sulfide can be calculated in a similar manner according to:

$$H_2S = H_2 + \frac{1}{2}S_2 \rightarrow p_{S_2} = K * \left(\frac{p_{H_2S}}{p_{H_2}} \right)^2 \quad (2.5)$$

K Equilibrium constant ($\Delta G^0 = -R * T * \ln(K)$)

Again, with the calculated partial pressure and the standard Gibbs free energy of formation it is possible to determine the stability of the metal sulfides.[12]

The same procedure applies for the formation of metal chlorides in a chloridising atmosphere.[12]

2.2 Corrosion kinetics in gases

Knowledge of the thermodynamics of a reaction allows to predict whether this reaction generally takes place or not, but it does not contain any information about how fast the reaction will be. Therefore, knowledge of the kinetics of a reaction is likewise required.[13]

If metals are able to be oxidized, they can be classified into the ones that form a protective oxide layer and those that cannot, according to Pilling and Bedworth [14]. In case of aluminium, as an example, the oxidation proceeds according to equation 2.6:



So the Pilling-Bedworth ratio results in:

$$\frac{\text{Volume of 1mol of } Al_2O_3}{\text{Volume of 2mol of Al}} \quad (2.7)$$

With equation 2.7 it is possible to estimate the protection of the resulting oxide layer. In case of a ratio <1 the formed oxide layer will be porous and contains cracks, therefore it is not protective. If the ratio in equation 2.7 is >1, the oxide scale is protective and the oxidation only can proceed due to slow solid-state diffusion, even at high temperatures. If the ratio is higher than 2, rapid growth of the oxide scale leads to compressive stress in the layer, and therefore it is possible that the scale spalls off. Although this theory has its exceptions and limitations, it is a helpful rule-of-thumb to get information about the forming oxide scale.[11]

If the Pilling-Bedworth ratio is <1 , the reaction rate of the oxidation remains constant over time, expressed by a linear oxidation rate:

$$\frac{dx}{dt} = k_L \quad (2.8)$$

x Mass [kg] or thickness [m] of the formed oxide

t Time of oxidation [s]

k_L Linear rate constant [kg/s] or [m/s] (function of the metal, gas composition and pressure, and temperature)

After integration equation 2.8 results in:

$$x = k_L * t \quad (2.9)$$

An example for such a linear kinetic behaviour is the oxidation at very high temperatures. Under such conditions the diffusion process through the porous oxide layer in the scale is so fast, that it does not affect the oxidation rate. In this case the oxidation will proceed until the metal will be destroyed. A schematic representation of such a linear oxidation rate is shown in Figure 2.1.

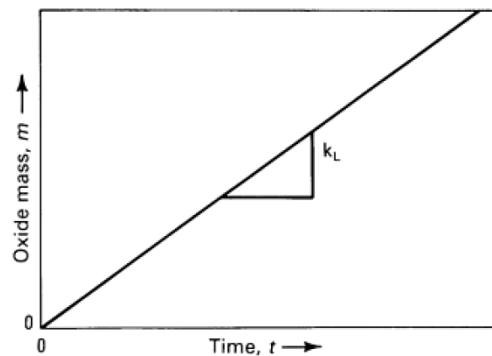


Figure 2.1 Linear oxidation rate [11]

If the oxide layer is very thin and the temperature low, the corrosion rate normally follows a logarithmic (equation 2.10) or inverse logarithmic (equation 2.11) reaction rate:

$$x = k_e * \log(a * t + 1) \quad (2.10)$$

$$\frac{1}{x} = b - k_i * \log(t) \quad (2.11)$$

a, b, k_e, k_i Constants

In Figure 2.2 the logarithmic and inverse logarithmic kinetics are shown.

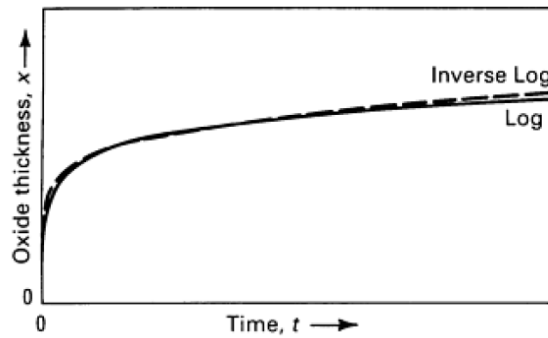


Figure 2.2 Logarithmic and inverse logarithmic oxidation rate [11]

Under the conditions of a thin oxide scale, electrostatic effects have the main influence on the mass transfer through the scale. The oxidation, according to the logarithmic and inverse logarithmic law, proceeds until a limiting scale thickness is reached. As shown in Figure 2.2 both rate laws lead to nearly identical results. Experimentally, it is also very difficult to distinguish between the two laws, because of the complex conditions caused by the thin oxide scale.[11]

Another rate law is valid if the rate-limiting process of the oxidation is related to the diffusion of the ions through the oxide layer, and the driving force is the gradient of the chemical potential. Under these conditions the rate slows down with increasing layer thickness.

$$x^2 = k_p * t \quad (2.12)$$

k_p rate constant [kg^2/s] or [m^2/s]

This type of oxidation rate has parabolic kinetics and it appears on metals that form a compact oxide layer. A graphical representation is shown in Figure 2.3.

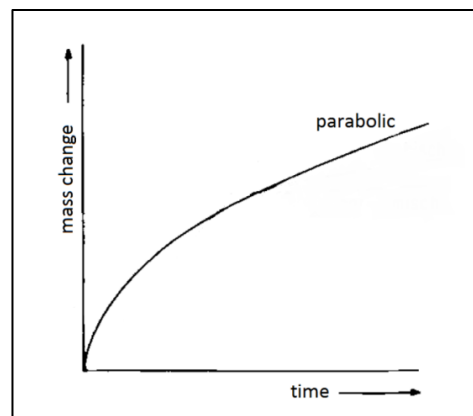


Figure 2.3 Parabolic oxidation rate [12]

If the oxidation rate is controlled by diffusion it can be described with Fick's first law.

For the diffusion rate in one dimension and a system with constant temperature and pressure it results in:

$$J = -D \frac{\partial C}{\partial x} \quad (2.13)$$

J Flux [mol/(s*m²)]

D Diffusion coefficient [m²/s]

C Concentration of a component [mol/m³]

For the diffusion through the oxide scale equation 2.13 can be approximated by the difference of the concentrations at the scale-gas and scale-metal interfaces. This leads to equation 2.14:

$$J = -D \frac{\Delta C}{\Delta x} = \frac{-D(C_2 - C_1)}{X} \quad (2.14)$$

The corresponding graphical representation is shown in Figure 2.4.

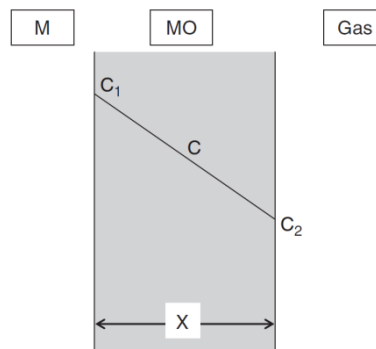


Figure 2.4 Diffusion model for mass transport through metal oxide (MO) scale [15]

Besides the linear oxidation rate all other oxidation kinetics lead to rapid oxide scale growth at the beginning followed by a much slower oxidation rate with increasing time.[11, 12, 15]

2.3 Corrosion

According to DIN EN ISO 8044 [16] corrosion is generally defined as the “*physiochemical interaction between a metal and its environment that results in changes in the properties of the metal, and which may lead to significant impairment of the function of the metal, the environment, or the technical system, of which these form a part*”. Metals can be affected by a lot of different types of corrosion. The main difference between those corrosion types is connected with the surrounding environment. This can be an aqueous solution, a non-aqueous liquid or a gas. In case of a gas the corrosion mechanism is chemical. The corrosion in a non-aqueous liquid has a metal-physical mechanism, and if the environment is an aqueous solution the corrosion has an electrochemical nature.[12] The requirements for

such an electrochemical corrosion are an existing electrolyte, the possibility to form an anode and a cathode and an electrical conduction between the two formed electrodes. At the anode the metal is oxidised. The so formed metal ions are dissolved and the electrons diffuse through the electrical connection to the cathode. In Figure 2.5 a schematic representation of a corrosion cell is shown.[17, 18]

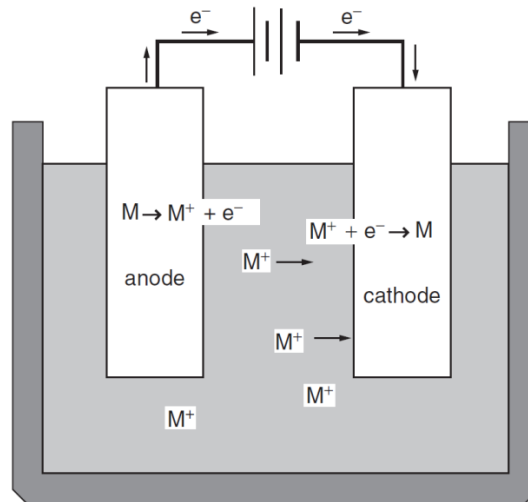


Figure 2.5 Corrosion cell [17]

The galvanic series ranks the metal nobilities and describes whether a metal acts as cathode or anode. The most noble metal stands on the top of the list. The order, however, can change due to different testing environments (e.g. pH, concentration, temperature). The most common testing environment is seawater. In this list graphite has the highest nobility.[18]

2.4 High-temperature corrosion

High-temperature corrosion occurs at temperatures where aqueous electrolytes do not exist. The material damage at high-temperature corrosion is mainly due to constant material loss and crack initiation, followed by leakage, hot forced rupture, etc.[12] There are numerous different corrosion types, but the main ones are high-temperature corrosion in gaseous atmosphere, high-temperature corrosion in molten salts and corrosion under hot depositions.[12, 19] The focus of the master thesis lies on the high-temperature corrosion in certain gaseous atmospheres. Therefore the other two types will not be discussed.

Depending on the existing gaseous environment, different types of attack are possible: oxidation, carburisation, sulfidation, chlorination.[11] In most cases the corrosive attack does not take place only due to one aggressive component but in various combinations thereof.[12]

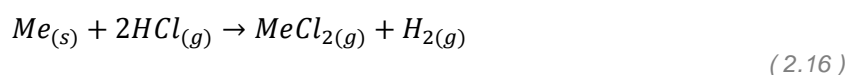
Corrosion in gases is an example for a chemical reaction with a redox character. A redox reaction describes the increase of the oxidation state of the metals and alloys in any reaction and the reduction of the gaseous components, which means a decrease of the oxidation

number. This can lead to oxides, sulfides, chlorides, etc.[20] The presence of chlorine, hydrogen chloride or other chlorides in the gaseous atmosphere can accelerate other types of corrosion, like sulfidation, depending on the temperature. The chloride breaks down the oxide layer and simplifies the access to the metal surface for other species such as H₂S.[6, 21]

2.5 High-temperature chlorine-induced corrosion

There can be different types of atmospheres in which the chlorine corrosion of metals occurs. One of those differences is the oxygen partial pressure (p_{O_2}). The higher the oxygen partial pressure is, the higher the oxidising character of this gas atmosphere will be. If no or only little reactive oxygen is available, p_{O_2} consequently is low and the gas atmosphere becomes reducing. The presence of oxygen and the combined variation of the oxygen partial pressure lead to aberrations in the corrosion mechanism of different metals in an HCl-containing environment.[22]

Nevertheless, the initiation of the corrosive attack is the same in both HCl atmospheres (with and without O₂). Hydrogen chloride is able to diffuse through the natural oxide scale of the metal.[6] As soon as the hydrogen chloride reaches the oxide-metal-interface it can react with iron and other alloying elements and form metal chlorides according to equations 2.15 and 2.16. The metals Fe, Cr and Ni show significant differences in their reaction with HCl, that are caused by their different vapour pressures and different likelihood to form chlorides and oxides. The formation of metal chlorides takes place according to their Gibbs free energies of formation, which are at 600 °C: CrCl₂ = -286.0 kJ/mol; FeCl₂ = -232.1 kJ/mol; NiCl₂ = -174.2 kJ/mol. Therefore chromium chloride will form more likely than iron chloride followed by nickel chloride.[1] Depending on the vapour pressures of the metal chlorides, they will evaporate more or less easily at temperatures above 400 °C (equation 2.17). Iron(II) chloride, for example, has a high vapour pressure and therefore will evaporate constantly whereas chromium(II) chloride needs much higher temperatures to evaporate, compared to iron(II) chloride at the same vapour pressure.[1, 21] Figure 2.6 shows the vapour pressures controlled by the temperatures.



'Me' stands for the metals Fe, Cr or Ni.

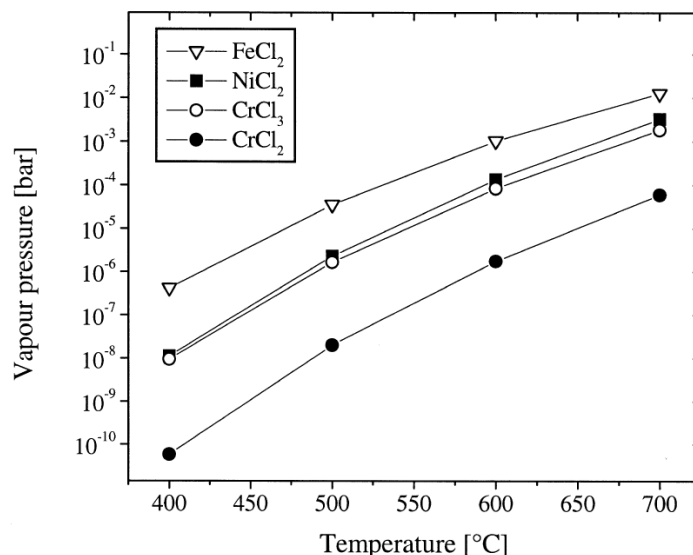


Figure 2.6 Temperature dependence of equilibrium vapour pressures of solid metal chlorides [1]

Because of their high vapour pressures, the gaseous metal chlorides will diffuse to the surface of the scale. The likelihood of evaporation is as following: $\text{FeCl}_2 > \text{NiCl}_2 > \text{CrCl}_2$. [1] The described processes apply to atmospheres with only HCl as well as the environment of the metal with additional O_2 . The following reactions of the different metals Fe, Cr and Ni and their corresponding metal chlorides, however, proceed differently depending on the atmosphere. The metal chlorides can be carried away with the passing gas stream, converted into oxides or stay in the corrosion layer. Thus, the atmospheres with and without oxygen will be discussed separately.

2.5.1 Corrosion in gaseous HCl without O_2

In pure HCl gas, iron shows a nearly parabolic rate law until a temperature of about 450 °C, due to the formation of a FeCl_2 corrosion layer. At higher temperatures the evaporation of FeCl_2 starts and proceeds simultaneously with the formation of new FeCl_2 . If the temperature rises even more, the metal will suffer from rapid mass loss because of the accelerated formation and evaporation of FeCl_2 . The corrosion of iron at higher temperatures will follow a linear rate law. Further chlorination of FeCl_2 to FeCl_3 with HCl as source, however, is thermodynamically impossible in a pure HCl atmosphere without any oxygen. [23]

The corrosion of chromium in pure HCl gas will proceed similar to the one on iron. Chromium forms likewise a CrCl_2 layer. However, for chromium compared to iron, a much lower mass loss takes place at the same temperature. [1] This can be explained with the lower vapour pressure of CrCl_2 . Up to 600 °C the corrosion rate will be nearly parabolic and decreases with time due to the increasing layer thickness and therefore inhibited diffusion. If the temperature reaches more than 600 °C, CrCl_2 starts to evaporate, and the formed CrCl_2 layer then is not protective any longer. The mass loss increases due to facilitated corrosion. [24]

Nickel is one of the most resisting metals in case of chlorine corrosion. Compared to FeCl_2 and CrCl_2 , NiCl_2 has a rather high Gibbs free energy of formation. Hence, in alloys containing a mixture of Fe, Cr and Ni, nickel will be the last element to react with HCl. At temperatures up to 400 °C and an atmosphere containing HCl vapour, solid nickel chlorides grow on the pure nickel substrate. Therefore the rate limiting factor is the diffusion process in solid NiCl_2 , and the reaction rate can be described with a parabolic law. With rising temperature the evaporation of NiCl_2 , which is controlled by the diffusion of the NiCl_2 through the laminar diffusion boundary layer, becomes important. The metal loss occurs due to the steady growth of the layer thickness and the constant evaporation of NiCl_2 . If the temperature is even more increased, the stability of solid NiCl_2 decreases, and it is possible that only gaseous NiCl_2 exists. In this case two limiting factors are valid: The diffusion of Cl_2 / HCl from the passing gas stream through the laminar diffusion boundary layer or the diffusion of gaseous NiCl_2 into the passing atmosphere.[12]

A schematic overview of the different processes during chlorine-induced corrosion in hot HCl atmospheres of different metals is shown in Figure 2.7.[12]

Without the presence of oxygen, no metal oxides can be formed and the mass loss is related to formation and evaporation of MeCl_2 . Further chlorination of the different MeCl_2 phases into MeCl_3 with HCl only and without any oxygen is thermodynamically impossible, too. This becomes advantageous at lower temperatures because MeCl_2 phases have a lower vapour pressure compared to MeCl_3 . Therefore evaporation of MeCl_2 phases starts at higher temperatures than those of the more volatile MeCl_3 phases. [23-25]

Iron has the fastest corrosion rate compared to chromium and nickel, due to the combination of a low Gibbs free energy of formation and a high vapour pressure of iron(II) chloride. Additionally, an increasing mass loss of iron is strongly connected with rising temperature.[1]

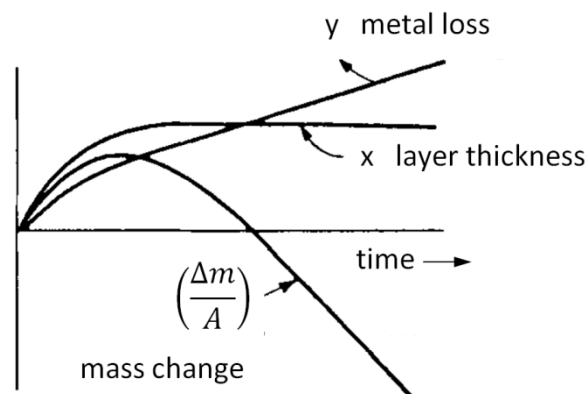
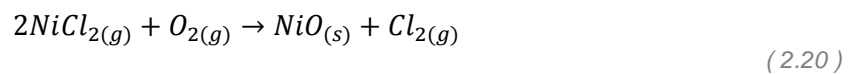
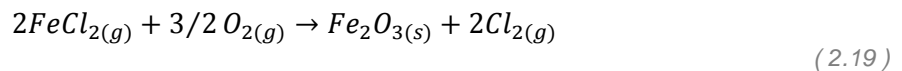
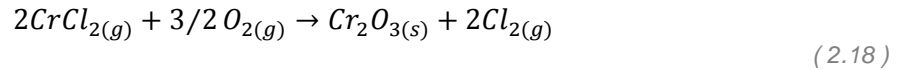


Figure 2.7 Schematic overview of the simultaneous growth and evaporation of the metal chlorides [12]

2.5.2 Corrosion in gaseous HCl with O_2

If the existing HCl atmosphere is oxidising, which means oxygen is present, the oxygen partial pressure becomes important. The thermodynamic stability of the formed metal

chlorides at a given temperature is controlled by the oxygen partial pressure. If the oxygen partial pressure is low enough, the metal chlorides can be formed and are the stable phase. In particular, this takes place at the oxide-metal-interface.[1] With increasing distance from the metal-oxide-interface, the oxygen partial pressure increases as well. As soon as the evaporated metal chlorides reach a region with adequate oxygen partial pressure, they will be converted into metal oxides, as it is shown in equations 2.18-2.20.[1, 21]



In each reaction chlorine is formed. This chlorine gas can be carried away with the gas flow or re-enter the oxide scale and react with the metal, according to equation 2.15. This mechanism of a constant formation of gaseous metal chlorides and their oxidation is named 'active oxidation'. It is an auto-catalysed process and leads to very loose and therefore non-protective oxide layers.[1, 6] Figure 2.8 shows a schematic overview of the 'active oxidation' process.

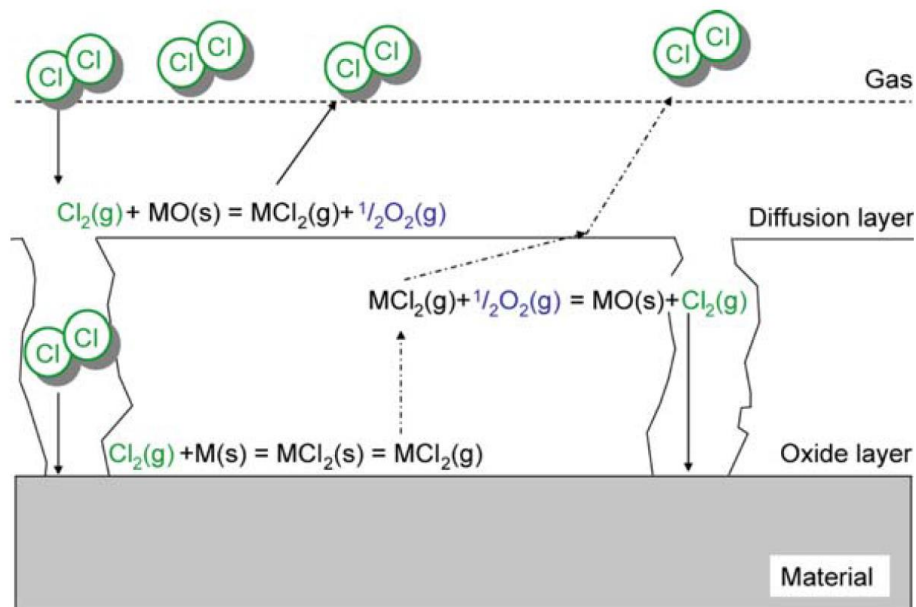
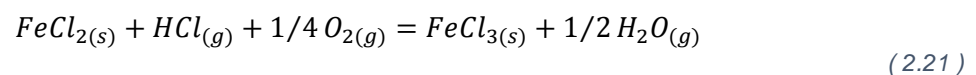
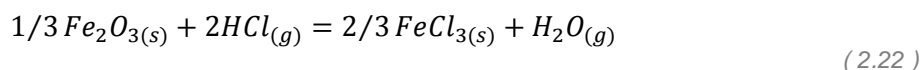


Figure 2.8 Schematic overview of the 'active oxidation' for a Cl_2 containing atmosphere [26]

In addition, the presence of oxygen in the atmosphere allows the so called oxy-chlorination to take place. In case of iron this leads to the formation of $FeCl_3$ according to equation 2.21.

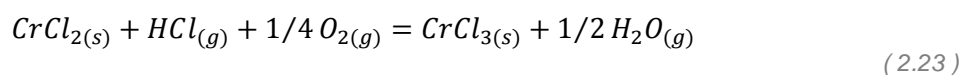


As noted above, in pure HCl gas the formation of FeCl₃ is thermodynamically impossible. However, FeCl₃ has a very low melting point (approx. 300 °C) and thus a high partial pressure at elevated temperatures. Therefore it evaporates more easily than FeCl₂. This is the main reason for the high corrosion rate of iron up to 400 °C in the gas mixture containing HCl and O₂. The corrosion rate increases with increasing temperature. In addition to the FeCl₃ formation, iron oxides can be formed, too. Normally, the formation of an oxide scale decreases the corrosion rate, but in a HCl / O₂ gas mixture these iron oxides lead also to the formation of FeCl₃ according to Equation 2.22. This takes place at temperatures between 300 °C and 400 °C and therefore accelerates the corrosion.



If the temperature rises up to 500 °C and more, the reaction according to equation 2.22 becomes thermodynamically unlikely. Therefore the possibility to form an oxide layer increases. Nevertheless, FeCl₃ can be formed simultaneously with Fe₂O₃ from FeCl₂ and HCl. Thus, the higher the oxygen partial pressure is the lower the corrosion rate will be. If the oxygen concentration increases, for example up to 75%, the corrosion rate can be decreased due to an increased oxide scale formation. The formed Fe₂O₃ layer is much less protective compared to other metal oxides, for example Cr₂O₃. Therefore iron will show severe damaging due to chlorine-induced corrosion.[23]

In case of pure chromium the corrosion in an atmosphere additionally containing O₂, will be decreased until a temperature of 500 °C because of the formation of a protective Cr₂O₃ layer. When the temperature exceeds 500 °C, an accelerated corrosion of chromium occurs because of the evaporating corrosion products. With oxygen present in the gas atmosphere it is possible to form CrCl₃ (equation 2.23), which has a higher vapour pressure compared to CrCl₂, as in case of iron.



This oxy-chlorination leads to the formation of a CrCl₃ layer beneath the Cr₂O₃ scale. If the oxygen concentration increases, the corrosion layer will mainly contain Cr₂O₃ and therefore decreases the corrosion rate.[24]

In case of nickel, the presence of O₂ in the atmosphere leads to nearly no change in the corrosion behaviour compared to the corrosion in a pure HCl atmosphere, because NiCl₂ is the thermodynamically favoured phase. Again, nickel compared to chromium and iron, is the most resistant metal against chlorine attack in the atmosphere with additionally oxygen.[25]

2.6 High-temperature sulfidation

The main problem caused by sulfidation is the reduction of the metal thickness due to formation of metal sulfides.[27] Sulfur is very common in petrochemical processes based on fossil fuels as feedstocks. It occurs as impurities in anthropogenic resources as well, due to biological components and therefore is present in combustion processes and the thermal cracking process. Sulfur operates as a very powerful oxidizing agent.[28] Sulfidation appears when metals or alloys get in contact with gas atmospheres containing S_2 , H_2S or SO_2 at high temperatures.[27] According to Mrowec [29] sulfidation not only takes place in atmospheres with high sulfur activity but also affects oxidation-resistant alloys in environments with low sulfur partial pressure. The likelihood of formation of the different metal sulfides is shown in Figure 2.9. The lowest line displays the most stable sulfide.[28]

Due to the higher number of defects in most sulfide layers compared to oxide layers, the diffusion coefficients are higher and therefore the diffusion can proceed way faster in sulfides than in oxides. Thus the growing rate of the sulfide scale is much higher, too.[12] Only for refractory metals the sulfidation rate is lower compared to the rate of oxidation because of the different defect concentration.[30]

According to Kunze [12] investigations with metals in sulfur vapour (S_2) showed that alloys with Fe, Cr and Ni as the main components had very fast sulfidation rates in such environments. However, in technical applications H_2S normally is present, instead of sulfur vapour. The sulfur partial pressure in atmospheres containing H_2S , H_2 , and hydrocarbons is specified due to the H_2S -/ H_2 -ratio. The sulfide layer normally grows fast whereas the sulfur transfer from H_2S is slow. Therefore the limiting factor for the sulfidation process will be the phase boundary reaction.

The reaction rate can be described with:

$$v = k * \frac{p_{H_2S}}{a_s} - k' * p_{H_2} \quad (2.24)$$

p_{H_2S}, p_{H_2}	Partial pressures [kg/(m*s ²)]
k, k'	Rate constants [(mol*s)/(m ² *kg)]
a_s	Sulfur activity [-]

The sulfur activity on the surface of the sulfide layer increases with increasing layer thickness. Therefore, according to equation 2.24, the sulfidation rate decreases with time until the sulfur activity on the surface is in equilibrium with the gas phase. This leads to non-linear kinetics, although the phase boundary reaction is the limiting factor which normally favours a linear reaction rate. According to this the sulfidation of iron can be tolerated between 300 °C and 400 °C.

An inhibition of the sulfidation can be achieved by adding silicium. This forms a Fe_3Si layer under the sulfide layer which inhibits the diffusion of iron to sulfur. Other inhibitors can act through the gas phase, like HCl or hydrocarbons. They influence the phase boundary reaction of the sulfur transfer. Chromium as an alloy can interfere the sulfidation as well, but only with a chromium content above 17wt.%. Chromium forms $(\text{Fe,Cr})\text{S}$ mixed sulfides, which will slow down the diffusion of the cations.[12]

Pure nickel shows only limited stability in sulfidising atmospheres. The formed sulfide layer is very porous, because the higher volume of the nickel sulfides compared to the corresponding oxides, leads to more spallation. In an atmosphere containing mainly H_2S pure nickel should only be used up to 320 °C. If the atmosphere is both oxidising and sulfidising the limiting temperature for nickel is about 370 °C.

In various industrial applications not only sulfur but mixed-gas atmospheres are present that typically contain oxygen (O_2 , CO , CO_2 , etc.) and depending on the process also HCl. Therefore not only sulfides but also oxides and chlorides can be formed.[12]

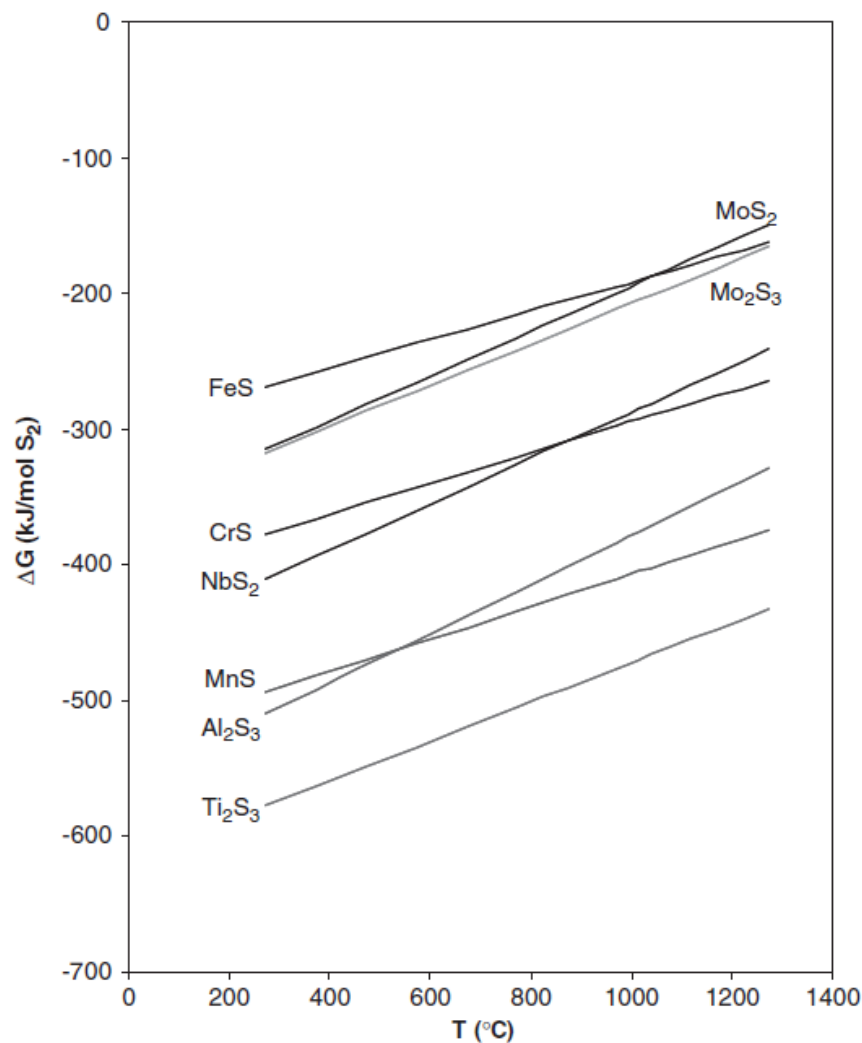


Figure 2.9 Ellingham diagram for selected sulfides [28]

2.7 High-temperature sulfidation and chlorination

The combination of sulfidation and chlorination occurs in some already mentioned processes, like coal gasification and thermal cracking of anthropogenic resources. In this case H_2S and HCl are present in the gas atmosphere. In coal gasification systems, for example, the composition of the produced syngas depends on the production process and the used coal. If the used fuel contains a certain amount of chlorine, HCl will be formed during the gasification process. The composition of the syngas normally adds up to the following components: CO , CO_2 , H_2 , H_2O , H_2S and HCl . The main problem in such a gasification atmosphere is the sulfidation and low alloyed steels suffer from severe corrosion by sulfidation. If the HCl content is in the range of 100-600 ppm in a highly reducing atmosphere and at temperatures around 450 °C it does not increase the corrosion rate of the low alloyed steels. Nevertheless, the sulfidation rate of those low alloyed steels is too high, and therefore they cannot be used in production.[31] More specific tests were made by Bakker and Perkins.[10] They added 600 ppm HCl to a syngas containing 0.6wt.% H_2S at a temperature of 350 °C. The results revealed a severe reduction of the sulfidation rate of low alloyed steels. Other authors published a decreasing corrosion rate in the temperature range of 200 to 399 °C when H_2S was added to the HCl -containing atmosphere.[10]

However, according to Haanappel [32] the addition of chlorine into a sulfidising-oxidising atmosphere increases the corrosion rate of the low alloyed steel after all. Pan et. al.[2] also reported that an increase of the H_2S concentration in an gas mixture containing HCl , H_2 and CO_2 at a temperature of 600 °C accelerated the corrosion rate of chromium-alloyed steels with a chromium content of 8, 12, 18wt.%.

In case of higher alloyed steels with chromium contents above 20wt.% the corrosion in sulfidising atmospheres not only depends on the p_{S_2}/p_{O_2} ratio but also on the HCl content. The mass loss under pure high temperature sulfurizing conditions normally is low enough to be handled with long term service. In atmospheres where HCl is present, the corrosion rate increases with decreasing chromium content because of a protective $FeCr_2S_4$ layer is not formed, followed by scale spallation.[31]

3 Methods of analysis

To analyse the corrosion of the different metal samples not only the mass loss is important but also the chemical reactions of the metal and on the metal surface. The corresponding chemical processes can be evaluated by investigating the corrosion products with SEM (scanning electron microscopy) / EDX (energy-dispersive X-ray spectroscopy). Additionally, XRD (X-ray powder diffraction) analysis provides information about the (phase) composition of the corrosion products.

3.1 SEM / EDX

For scanning electron microscopy (SEM) the surface of the sample is scanned with an electron beam. This leads to interactions between the sample surface and the electrons which can be used to create a picture of the surface. The whole process must be performed under high vacuum, otherwise the electrons would be disturbed by gas molecules. The source for the electron beam was a LaBa₆ cathode. The advantages of SEM are high-resolution images and the possibility to provide chemical analyses of the sample surface by energy-dispersive X-ray spectroscopy (EDX). In this method the atoms of the sample interact with the electron beam and send out X-ray-radiation. Every atom has a specific radiation (wavelength) which provides the information about the composition of the sample. [33, 34] The SEM / EDX instrument used for the analyses in this work was from Zeiss (EVO MA 25 ®).

3.2 XRD

X-ray powder diffraction (XRD) is a technique to analyse crystalline materials. It is a non-destructive and rapid method to characterise such materials. The structural information is preserved in the position, intensity and shape of the received diffraction peak. Each crystal structure has a characteristic diffraction pattern, which leads to the identification of the single components of the sample (phase analysis). To simplify this process of diffraction, the structure of the crystal is described as a compound built of layers, also known as lattice-planes. Those lattice-planes can be mathematical characterised with the indices (h k l). If an X-ray beam reaches a lattice-plane, one part gets reflected and the other part goes through it to the next lattice-plane and gets reflected there. For diffraction, the X-ray beams must interfere positively.

The relation between lattice planes, diffraction angle and used wavelength is expressed by the Bragg equation (3.1):

$$2d * \sin\theta = n * \lambda \quad (3.1)$$

- d Vertical distance between two lattice-planes [Å]
- θ Diffraction angle [Å]
- n Order of diffraction
- λ Wavelength of the used X-ray beams [Å]

For one given lattice-plane-band more different orders of diffraction can exist.[34]

The XRD analysis needs monochromatic beams. For the production of monochromatic beams the strong K_{α} -radiation is used. To erase other wavelengths, like the K_{β} -radiation, the K_{α} -radiation needs to be filtered. Another way to get monochromatic beams is due to a single-crystal-monochromator. [34, 35]

The XRD used for the measurements was a PanAlytical X'Pert Pro diffractometer with $\text{CuK}_{\alpha 1,2}$ radiation (1.54060Å, 1.54439Å). The scan length was 2.546° in the 2θ range 5-70° and an exposure time of 10s per scan length.

4 Experimental procedure

The used testing application was planned and built up by Alexander Schmid.[36] The two gas bottles are placed in a locker right next to the extractor hood in which the other testing equipment is located. On each gas bottle a pressure reducing valve is attached to regulate the pressure in the following pipeline. Before the gas enters the silica glass tube, the gas stream has to be regulated to a constant mass flow of about 120 ml/min. This is accomplished by a rotameter for each gas bottle. After the specific gas flow passes the rotameter, it gets merged from two separate pipelines into one. A flange connects the pipe with the silica glass tube. At the exit of the silica glass tube the reaction gases are led into a gas washing system filled with NaOH solution. This is required to neutralize the excessive parts of HCl and H₂S in the gas stream. The now cleaned gas stream can be led into the extractor hood, where it will be exhausted. The silica glass tube with the samples is heated with a tube furnace, manufactured by Carbolite-Gero. A schematic representation and a photograph of the pilot plant are displayed in Figures 4.1 and 4.2.

Due to a temperature gradient in the tube furnace it was necessary to determine the temperature at the sample position with an external thermocouple before the experiments. The calibration curve of the furnace is shown Figure 4.3.

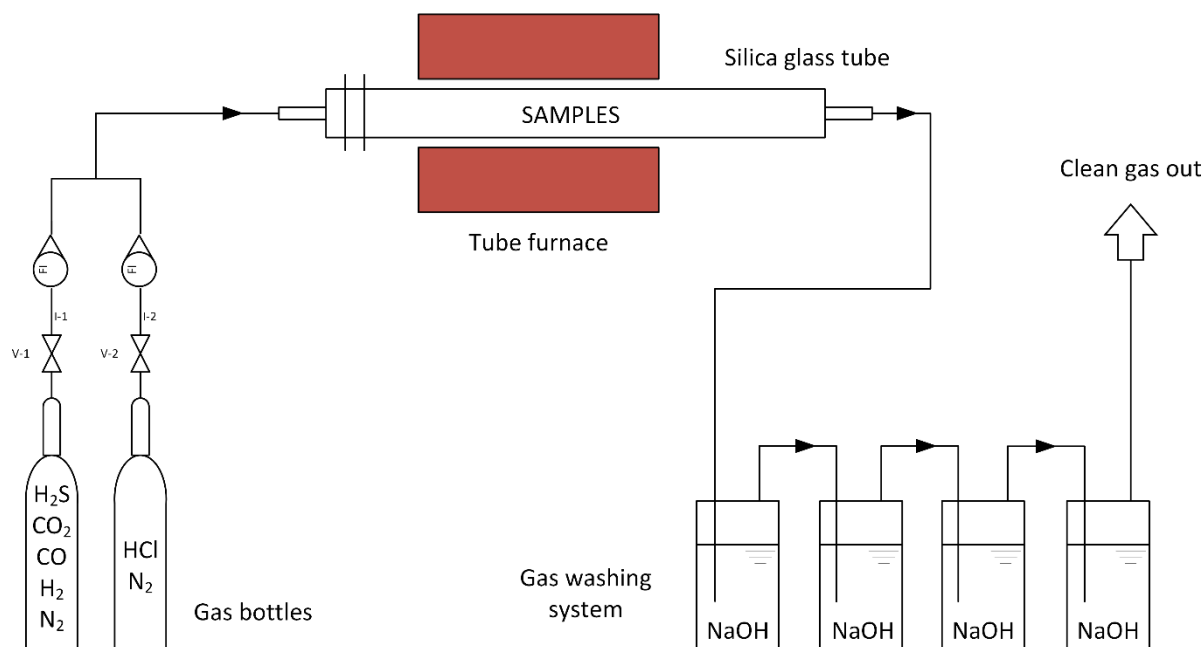


Figure 4.1 Scheme of the testing equipment



Figure 4.2 Experimental setup

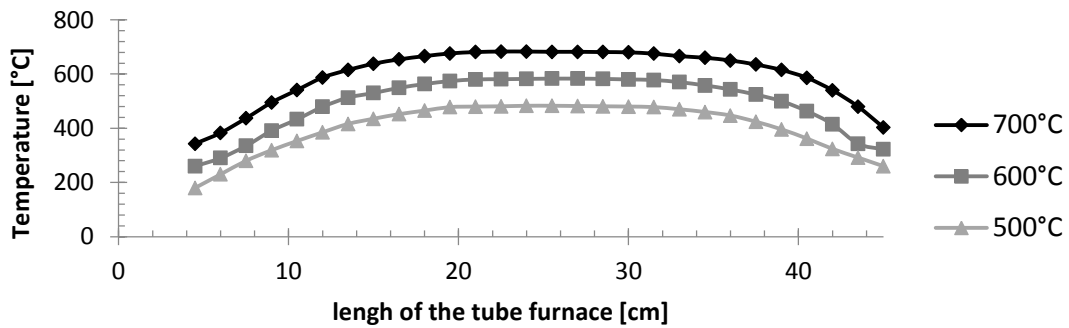


Figure 4.3 Real furnace temperatures

To get information about the influence of the alloying elements during the corrosion process, two different iron-based alloys were tested. The chemical composition of both alloys and the dimensions of the samples are shown in Table 4.1 and 4.2.

Table 4.1 Chemical composition of the used iron alloys according to the manufacturer in wt.%

	Fe	Ni	Cr	C	Si	Mn	P	S	Ti	Al
P9 steel	bal.	-	9	0,1	0,5	0,5	-	-	-	-
Alloy 800HT	bal.	30	20,5	0,07	0,6	0,6	≤0,025	≤0,010	0,5	0,5

Table 4.2 Dimensions of the samples

		[mm]	
Length	l	25	
Width	b	10	
height	h	2	

The P9 steel was provided by Voest Alpine Tubulas and is also known as 1.7386. It has a ferritic structure. Normally this steel is used as superheater pipes and header.

Alloy 800HT, also known as 1.4959, was provided by Sandvik. It has an austenitic structure and is an iron-nickel-chromium alloy. It has very good high temperature corrosion resistance and is much more expensive than P9 steel.

Prior to the corrosion experiments, all samples were grounded with 1000 grit SiC paper to ensure the same well defined surface. Subsequently, the samples were exposed to air atmosphere for at least 4 weeks to rebuild their natural oxide layer. Shortly before the actual corrosion experiments the samples were degreased with acetone, then gauged and weighed. Four specimens were placed in the silica glass tube during one test run into the gas stream without any interference between the single samples. They were positioned upright next to each other and facing the gas flow parallel to their biggest surface area (Figure 4.4).

The exact composition of the two testing gases is shown in Table 4.3.

Table 4.3 Composition of the test gases

	HCl	H ₂ S	CO ₂	CO	H ₂	N ₂
Test gas bottle 1	-	0,02vol%	0,3 vol%	1,9 vol%	2,8 vol%	bal.
Test gas bottle 2	3,8 vol%	-	-	-	-	bal.

The gases were provided by Linde gas (Eggendorf, AUT). To make sure that the gases have the same composition at every experiment, they were homogenised frequently. Nevertheless, it cannot be excluded that there are little aberrations in the gas composition during every experiment. The oxygen partial pressure under those conditions is very low and the chlorine potential relatively high.

The first round of tests was run with a 50:50 mixture of both gases, so that the corrosion under the combination of HCl and H₂S could be investigated. In the second round only H₂S and no HCl (100:0) was used as corrosive component, to see how the materials react in a sulfidising atmosphere without HCl. To have the same flow as in the 50:50 gas mixture (120 ml/min), nitrogen was added instead of HCl.

The different temperatures and periods applied during the experiments are listed in Table 4.4.

Table 4.4 Required temperatures and periods of the experiments

Temperature [°C]	Period [h]
480	24
580	72
680	240

In case of the 100:0 gas mixture, the tests were performed at temperatures of 480 °C and 680 °C for only 240 hours.

As already mentioned, four specimens can be placed into the gas flow during one experiment. Therefore a silica glass holder with four spaces was produced (Figure 4.4).



Figure 4.4 Silica glass holder without and with samples

Prior to the test phase, the specimens were placed into the silica glass pipe, and the pilot plant was purged with nitrogen for 30 minutes before and during the heating process. Once the required temperature was reached, the testing gases were added.

At the end of every experiment the gas bottles and the tube furnace were turned off. Again, the whole equipment was purged with nitrogen during the cooling, so all the corrosive gases were eliminated from the testing equipment. As soon as the furnace reached room temperature, the specimens could be removed.

To determine the mass losses, the samples were first cleaned with a wired brush in water to remove the loose corrosion products, followed by sonication (2 times for 30 seconds) in a 5% hydrochloric acid solution. This ensures all corrosion products to be removed. For control that this cleaning process only removes the corrosion products and does not attack the metal itself, a non-corroded P9 steel sample was put into the 5% hydrochloric acid in the ultrasonic bath and weighted before and after treatment for several times. Each measurement took 30 seconds. The mass loss was so small that it could be neglected (Figure 4.5).

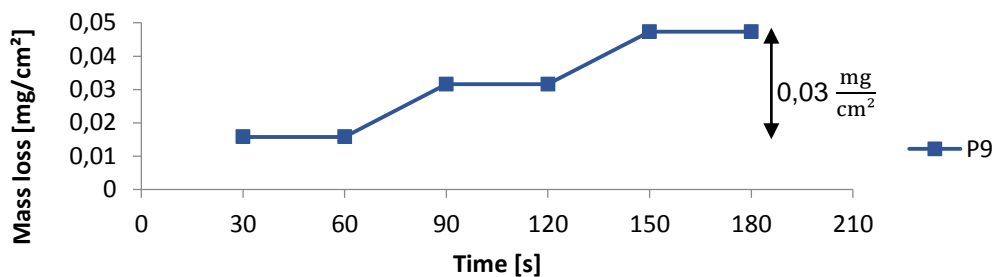


Figure 4.5 Mass loss of a non-corroded P9 steel sample in 5% HCl after several measurements of 30sec each

In addition, un-cleaned samples were cold mounted in epoxy resin. This had to be done right after the samples were removed from the furnace, so that water soluble corrosion products can be preserved and cross sections can be visualised unaltered. To investigate the cold

mounted samples with SEM / EDX analysis they had to be polished without water up to 3µm with diamond grit.

Furthermore, for the mass loss measurements cleaned specimens were hot mounted and polished up to 1µm. The samples then were etched to get a better view of the microstructure and the corrosion attack within the material. The used etchants were Beraha-I and -II. Beraha is a colour etchant. The stock solution consists of H₂O, HCl and (NH₄)HF₂, shortly before the etching K₂S₂O₅ is added. Beraha-I has a lower concentration and therefore is suitable for the lower alloyed P9 steel. Beraha-II is normally used for austenitic Fe-Cr-Ni steels and therefore applies for alloy 800HT. The polished and etched samples then got analysed with light microscopy.

5 Results and Discussion

5.1 Mass loss measurements

The mass loss for every sample was referred to its surface area. Figures 5.1-5.3 list the various mass losses for P9 steel and alloy 800HT at different temperatures in the 50:50 (with HCl and H₂S) gas mixture. After 24 hours (Figure 5.1) the mass loss of alloy 800HT did not change by increasing the temperature from 480 °C to 580 °C and only reached 1.7 mg/cm². Further increase of the temperature, up to 680 °C, led to a slightly increased mass loss of 3 mg/cm². With 2 mg/cm² after the experiment at 480 °C P9 steel showed nearly the same mass loss as alloy 800HT. At the higher temperatures, the mass losses increased to 9 mg/cm² at 580 °C and 105 mg/cm² at 680 °C.

After 72 hours (Figure 5.2) the mass loss of alloy 800HT decreased from 4.2 mg/cm² to 3 mg/cm² by increasing the temperature from 480 °C to 580 °C. The experiment at 680 °C led to a mass loss of 4.35 mg/cm², which is slightly higher than the one at 480 °C. P9 steel showed the same trend as for the experiments lasting 24 hours; the mass loss increased from 4 mg/cm² (480 °C) to 31.6 mg/cm² (580 °C). At 680 °C P9 steel had such a high mass loss (210 mg/cm²) that the sublimed iron(II) chloride, which re-crystallized in the colder part of the silica glass tube, nearly blocked the pipe (Figure 5.4). Therefore P9 steel was not tested in the 240 hours test run at a temperature of 680 °C.

Alloy 800HT showed a decreasing mass loss from 11 mg/cm² to 4.5 mg/cm² by increasing the testing temperature to 580 °C, after 240 hours. The mass loss of 4.5 mg/cm² at 580 °C was the same after the experiment at 680 °C. The mass loss of P9 steel after 240 hours at 480 °C reached a value of 9 mg/cm² and increased to 40 mg/cm² at 580 °C.

At the lowest testing temperature P9 steel showed the similar mass losses as alloy 800HT during all time slots. Alloy 800HT exhibits a more constant mass loss and especially at the highest testing temperature of 680 °C showed a very good resistance against the chlorine attack. The trend of the mass losses for each measurement time at the different temperatures remains nearly the same for alloy 800HT as well as for P9 steel. Only the mass loss and therefore the layer thickness increased with time.

Two parallel processes are interpreted to be responsible for the mass change of the samples. The first one is the formation and vaporisation of iron(II) chloride. This phase diffuses outwards through the corrosion layer and sublimates and/or gets carried away with the gas flow. In the colder part of the silica glass tube it then re-crystallizes. The second process involved in the mass change is the formation of sulfide and oxide layers. In a first step these reactions lead to an increase of the mass. At the cleaning process the corrosion products are removed and therefore contribute to the overall mass loss of the samples.

The mass loss of P9 steel highly increases with increasing temperature.

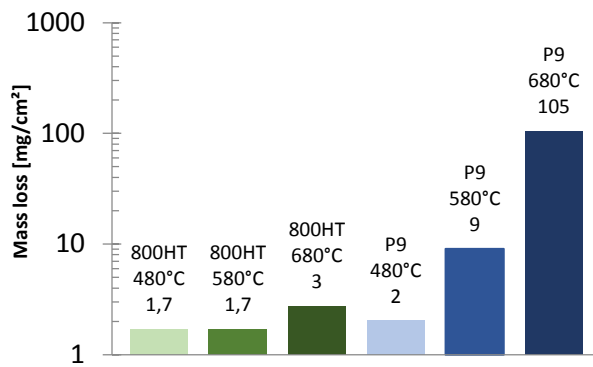


Figure 5.1 Mass loss of the alloys after 24 h at different temperatures

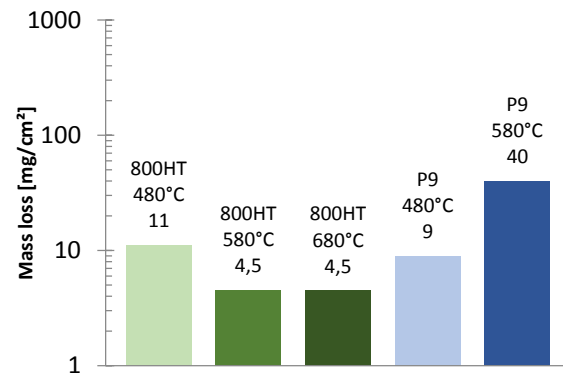


Figure 5.3 Mass loss of the alloys after 240 h at different temperatures

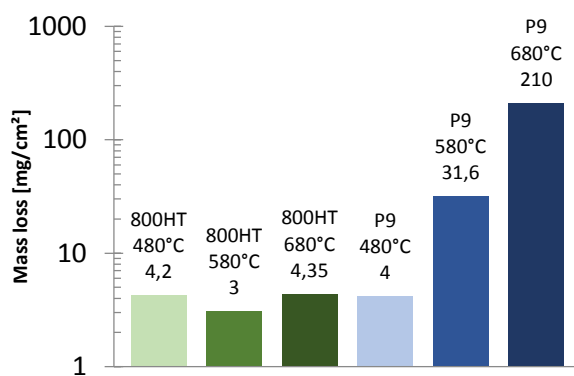


Figure 5.2 Mass loss of the alloys after 72 h at different temperatures

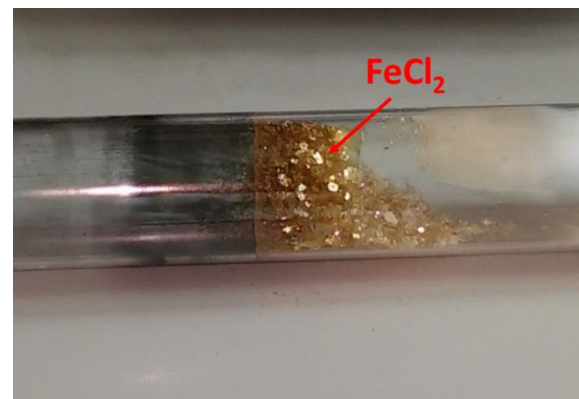


Figure 5.4 Iron(II) chloride in the colder part of the silica glass pipe

For the second part of the mass loss experiments, where H_2S is the only aggressive component, the results are listed in Figure 5.5. Alloy 800HT has a very low mass loss in the sulfidising atmosphere at both temperatures, compared to the P9 steel. At 480 °C the mass loss of alloy 800HT reached only 0.19 mg/cm², whereas for the P9 steel it was 23.8 mg/cm². After the experiment at 680 °C the mass loss of alloy 800HT increased to 1.16 mg/cm², but again was lower in comparison with the P9 steel, which showed a mass loss of 7.9 mg/cm². The mass loss of P9 steel decreased by increasing the temperature to 680 °C.

Figure 5.6 displays the results in the 100:0 mixture and in the mixed gas atmosphere with HCl (50:50). The mass loss of alloy 800HT in the 50:50 gas mixture was considerably higher than the one in the 100:0 atmosphere. P9 steel likewise suffers under severe sulfidation and at 480 °C shows a high mass loss compared to the environment with additional HCl. This matches with literature data. According to Kunze [12] HCl in the gas atmosphere can act as an inhibitor of the sulfidation process. Additionally, Bakker and Perkins [10] reported that the sulfidation of low alloyed steels can be reduced with HCl in the atmosphere at lower temperatures.

During the experiment at 680 °C the mass loss of P9 steel decreased compared to 480 °C due to sulfidation. This is the exact opposite behaviour than in the mixed gas atmosphere

where HCl was also present. The mass loss after 240 hours in the 50:50 mixture at 680 °C would be even higher than the one for 72 hours. This indicates that the high mass loss of P9 steel at the highest testing temperature in the 50:50 gas mixture is caused by HCl.

The main reason for the mass change during the experiments in the testing gas without HCl is the formation of a sulfide scale. Again, the formation of metal sulfides increases the mass of the sample, until they get removed during the cleaning process.

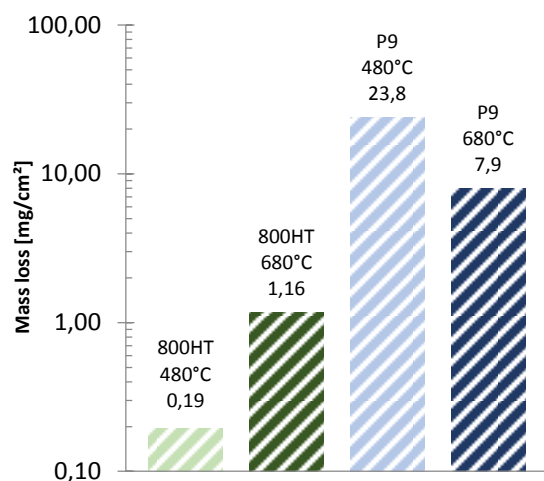


Figure 5.5 Mass loss of the alloys after 240 h in the 100:0 mixture at different temperatures

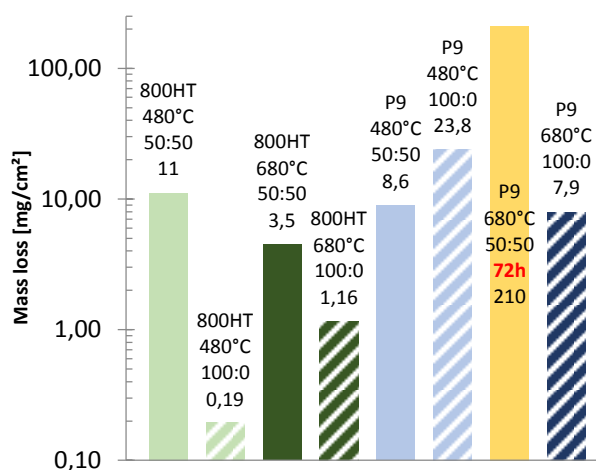


Figure 5.6 Comparison of the mass loss after 240 h in the 100:0 and 50:50 mixture and the mass loss of P9 after 72 h at 680 °C

To get information about the corrosion kinetics in the gas atmosphere with HCl at the different temperatures, kinetic curves were calculated. They are shown in Figures 5.7-5.9. Alloy 800HT shows a decreasing mass loss at all three temperatures with increasing time, which leads to a parabolic corrosion rate. This indicates the formation of a diffusion barrier and a limiting corrosion layer thickness. At the testing temperature of 680 °C the limiting layer thickness was achieved after 72 hours, due to no visible increase of the mass loss from 72 to 240 hours.

In case of P9 steel the corrosion rate shows parabolic kinetics, too, at temperatures of 480 °C and 580 °C. Due to the high mass loss at 680 °C the kinetic curve of P9 steel has only two measuring points and therefore no significant result to describe the corrosion rate. However, it can be assumed that the rate law would show a nearly linear character because of the very high mass loss after three days which indicates a very porous and non-protective layer of corrosion products that do not form an effective diffusion barrier.

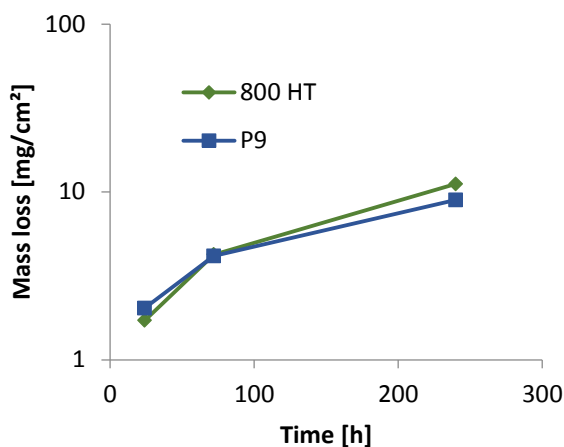


Figure 5.7 Kinetic curves at 480 °C from alloy 800HT and P9 steel after 24, 72 and 240 h

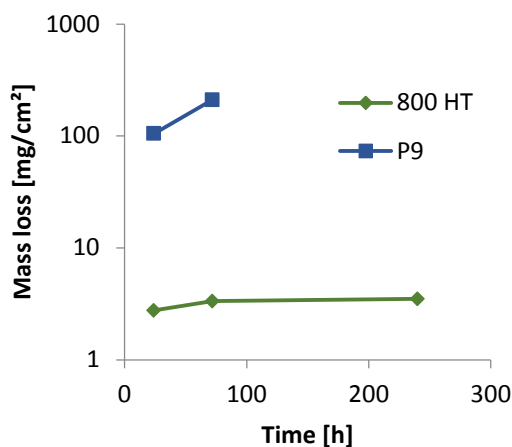


Figure 5.9 Kinetic curves at 680 °C from alloy 800HT and P9 steel after 24, 72 and 240 h

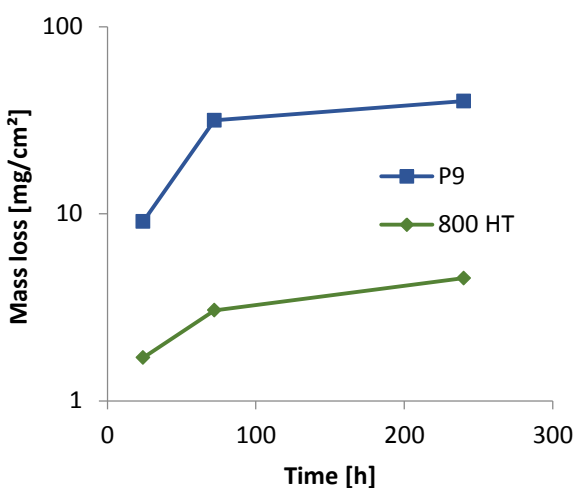


Figure 5.8 Kinetic curves at 580 °C from alloy 800HT and P9 steel after 24, 72 and 240 h

For the second part of the experiments with H₂S only, kinetic curves could not be derived because of the missing measuring points for the 24 and 72 hour measurements.

5.2 Corrosion products

5.2.1 Gas atmosphere with HCl

Nearly all tested samples showed a black layer of corrosion products. For both alloys at nearly all experiments in the gas atmosphere with HCl the layer was easy to remove and no further cleaning advises necessary. Independent of the different temperatures, the corrosion products of alloy 800HT were more loose compared to the ones on P9 steel. They spalled easily and could nearly completely be removed with a wired brush only. However, one exception occurred: At a temperature of 580 °C and a period of 10 days, the corrosion layer

on alloy 800HT was more adhere than after one and three days compared to P9 steel. It had to be cleaned for additional two times with 10% HCl to remove all corrosion products.

To get more information about the corrosion products and the corrosion mechanism, cross sections of the different samples with and without the corrosion layer were made. Selected cross sections were analysed with SEM / EDX and light microscopy. Furthermore thermodynamic calculations are beneficial to get information about the stability of the corrosion products in the test gas atmospheres.

Until the early 2000 years it was common to calculate phase stability diagrams for the occurring systems. This procedure was later disproved because phase stability diagrams are only valid if all formed corrosion products are either solid or liquid. The presence of chlorine in the gas atmosphere during the high-temperature corrosion leads to the formation of volatile metal chlorides that evaporate (especially in case of FeCl_2) above 400 °C. To get a valid diagram for prediction of the stability of corrosion product with all three possible phases (solid, liquid and gaseous), quasi-stability diagrams were introduced at that time. These diagrams are based on the stability line between oxide and metal and on the limiting vapour pressure of the volatile component. The common value for this limiting vapour pressure normally is 10^{-4} bar. Above this value it is assumed that severe mass loss of the metallic sample occurs due to evaporation of metal chlorides, whereas below 10^{-4} bar at least structural components should remain, because the evaporation of volatile metal chlorides is too slow.[26, 37, 38]

The introduction of the quasi-stability diagrams made it clear, that the previously used phase stability diagrams lead to an underestimation of the risk of chlorine-induced high-temperature corrosion.[26]

High-temperature corrosion shows a significant dependence on temperature. Therefore the corrosion products for each temperature will be discussed separately.

5.2.1.1 480 °C

The typical appearance of the samples after the lowest testing temperature of 480 °C is shown in Figures 5.10 and 5.12. There were no differences of the corrosion products for all three periods, only the thickness of the corrosion layer increased. The corrosion products on alloy 800HT show more spalling than the corrosion layer on P9 steel. In Figure 5.11 the reason why the samples had to be cold mounted immediately after they were removed from the furnace is visualized. The sample was exposed to the atmosphere only for a few minutes, before it was cleaned. The corrosion product on alloy 800HT after the experiment at 480 °C was very hygroscopic and changed its appearance completely. However, the pictured sample was cleaned and not mounted. Therefore the transformation of the corrosion products did not affect the results of further investigations.

In Figure 5.13 the resublimed FeCl_2 crystals are displayed. Compared to the higher temperatures only small amounts of iron(II) chloride were found in the colder part of the silica glass pipe, which indicates a lower mass loss due to slower vaporisation of FeCl_2 .



Figure 5.10 Alloy 800HT after 240 h at 480 °C in the gas atmosphere with HCl



Figure 5.12 P9 steel after 240 h at 480 °C in the gas atmosphere with HCl



Figure 5.11 Alloy 800HT after 240 h at 480 °C in the gas atmosphere with HCl, after exposure to ambient atmosphere



Figure 5.13 Re-crystallized FeCl_2 in the silica glass tube after 72 h at 480 °C

In Figure 5.14 the cross section of alloy 800HT after the experiment at 480 °C is depicted. A small gap separates the base material and the voluminous corrosion layer, which shows a multi-layered structure. The single layers of the corrosion products consist of a sulfide scale with a layer beneath it, formed out of an oxide-chloride-mixture. In the base material a material depletion occurs. According to EDX mappings of this sample (Figure 5.16), the main components of the single layers are iron chloride, iron sulfide, chromium oxide, and chromium sulfide. In case of chromium, this outcome does not match with the predictions of the thermodynamic calculations, because no chromium sulfide should exist under these conditions. The composition of the outer area of the corrosion layer, which reaches into the passing gas stream, differs from the other corrosion products. This layer mainly consists of nickel- and iron sulfides and nearly no chromium sulfides. The reason why nickel sulfides are

in the outermost layer is the comparable high affinity of nickel to sulfur. The metal diffuses towards a higher sulfur concentration and in addition, does not react with HCl or H₂O and therefore is not converted into oxides or chlorides. NiS in the outer area of the corrosion layer is responsible for the different appearance of the sample shown in Figure 5.11. When exposed to air NiS is oxidized and converts to Ni(OH)S, which leads to an increased volume.[39] The sulfide layer is in any case located above the oxide/chloride scale. The base material suffered from an irregular material abrasion. Beneath this area with accompanied material loss nickel was enriched. This implies that nickel is the least reactive metal in the row, and therefore has a higher probability to remain in the base material in comparison with iron and chromium. It should be noted that the high chlorine concentration pictured in the mapping does not reflect the reality. Isopropanol, which was used during the polishing, dissolves and or leaches (parts of) the metal chlorides and moves into the holes of the corrosion layer. The solvent then evaporates and leaves the metal chlorides in the holes of the corrosion layer, thus leading to an artificial enrichment of chlorine.

The cross section of P9 steel is shown in Figure 5.15. In comparison with alloy 800HT, the corrosion layer of P9 steel has a more irregular appearance. The gap, which separates the corrosion layer from the base material, is about 40 µm and therefore considerably thicker. The outer layer is thick and voluminous. The inner layer, which is only a few micrometres high, does not contain corrosion products. We assume that those areas developed during the grinding process. The base material suffers under a comparable constant material abrasion and does not show significant material depletion, which indicates a loss of the main components, viz. iron and chromium. In Figure 5.17 the EDX mapping of P9 steel after 240 hours at 480 °C is shown. The outer layer, which reaches into the gas stream, consists of sulfur, chlorine, iron and chromium, with iron(II) chloride, iron sulfide, chromium sulfide and chromium oxide, as the most likely phases to be formed. The main constituent in the corrosion products are chlorides which are formed by the reaction of HCl with iron or chromium. Some amount of FeCl₂ also get carried away with the passing gas stream and resublime in the colder part of the silica glass pipe, visible as colourless crystals. Another part of iron chloride is converted into sulfides. On the other hand, chromium chlorides mostly convert into sulfides and some oxides. Normally, such sulfides are in the outer part of the corrosion layer, but here they are under a layer of FeCl₂. This outer iron chloride scale probably is formed during the cooling process or present because of the comparable low temperature that was not high enough to cause a complete evaporation of FeCl₂.

Areas with high chlorine concentration in the mapping partly match with a high carbon concentration. This indicates an area (hole) where the epoxy resin filled up these spaces, but left enough pores so that isopropanol, infiltrate these voids (see above). During evaporation of the solvent, metal chlorides are transported to the surface, due to capillary action which

can be seen in the mapping. However, these areas with a high chloride concentration do not represent corrosion products. The same applies for areas with a high oxygen concentration. The transported metal chlorides were oxidized by oxygen present in the surrounding atmosphere. Hence, these areas do not represent real corrosion products.

Other areas with a high oxygen concentration which do not match with areas with a high carbon concentration as shown in the mapping, are most likely Cr_2O_3 .

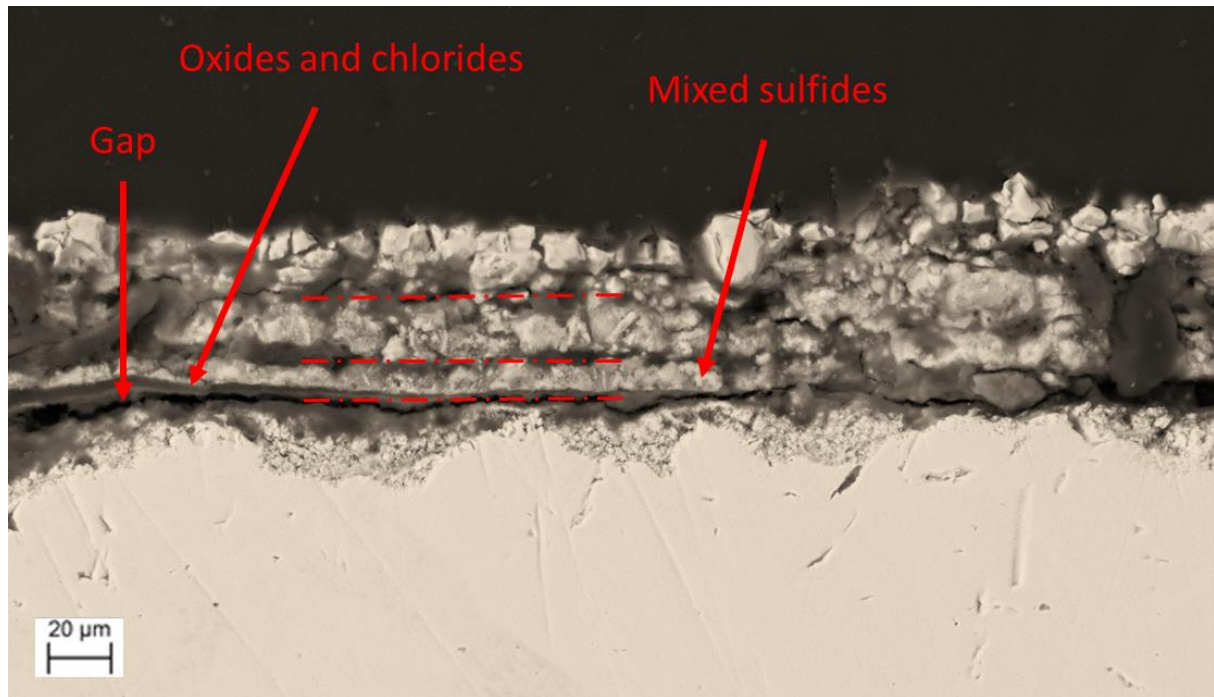


Figure 5.14 Cross section of alloy 800HT at 480 °C after 240 h in the 50:50 gas mixture

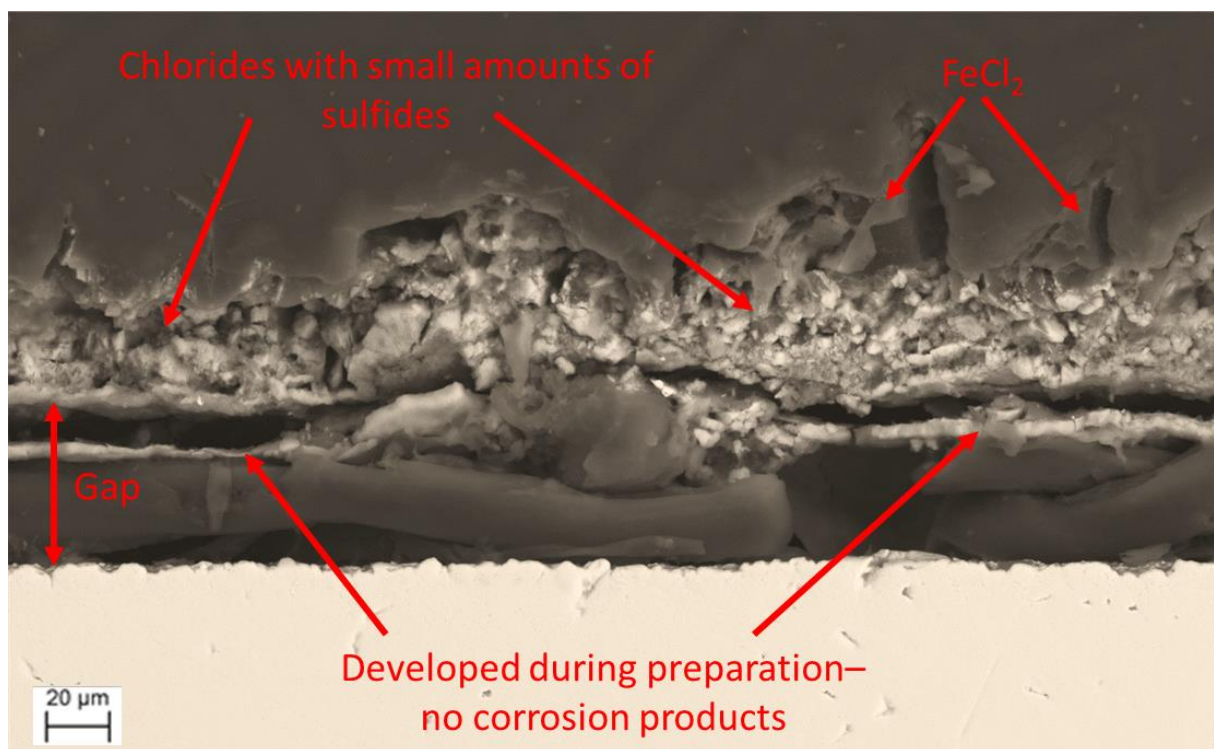


Figure 5.15 Cross section of the P9 steel at 480 °C after 240 h in the 50:50 gas mixture

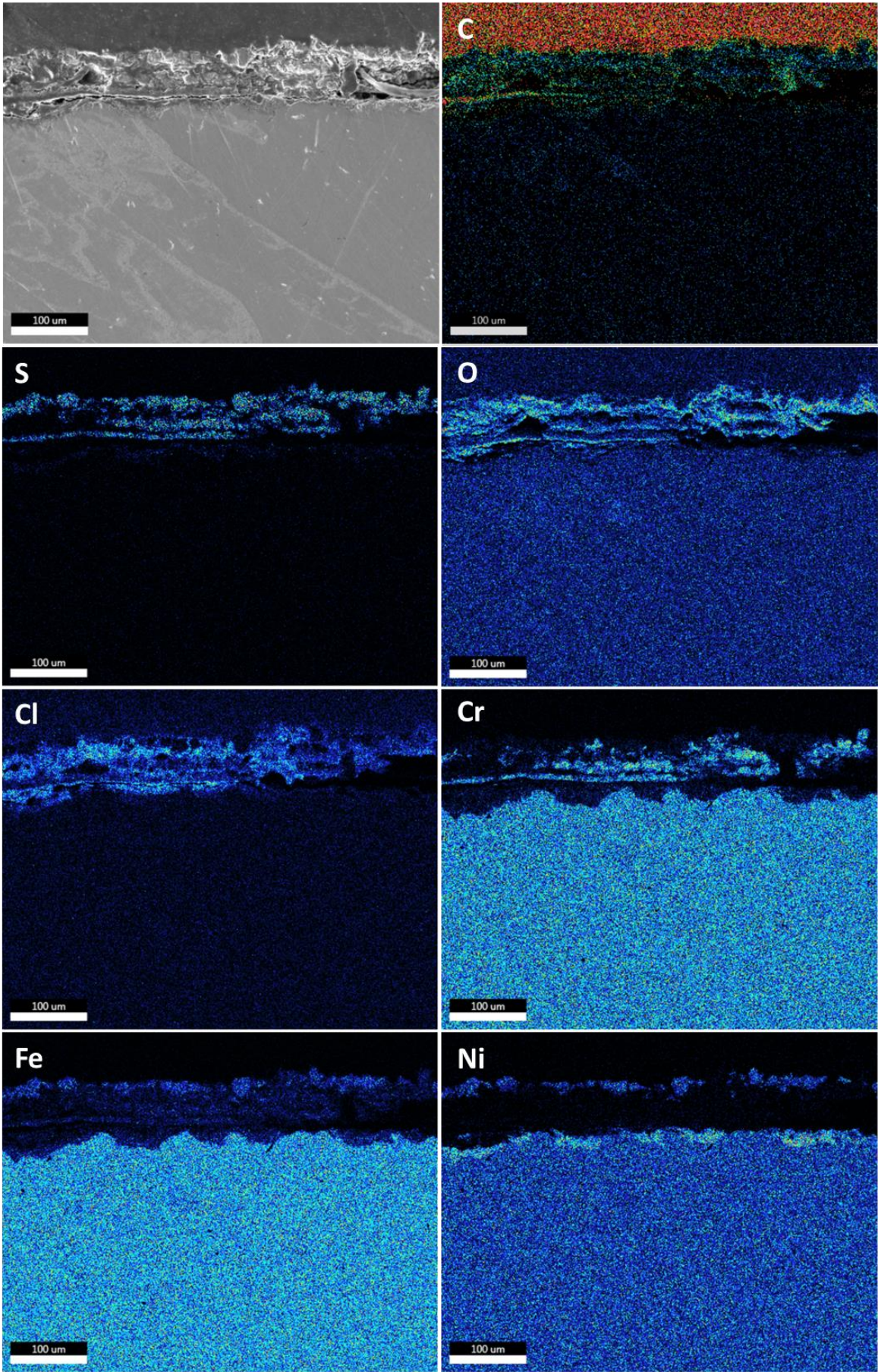


Figure 5.16 EDX mapping of a cross section of alloy 800HT at 480 °C after 240 h in the 50:50 mixture. The colour is connected with the concentration and increases from dark blue, light blue, green, yellow, orange to red.

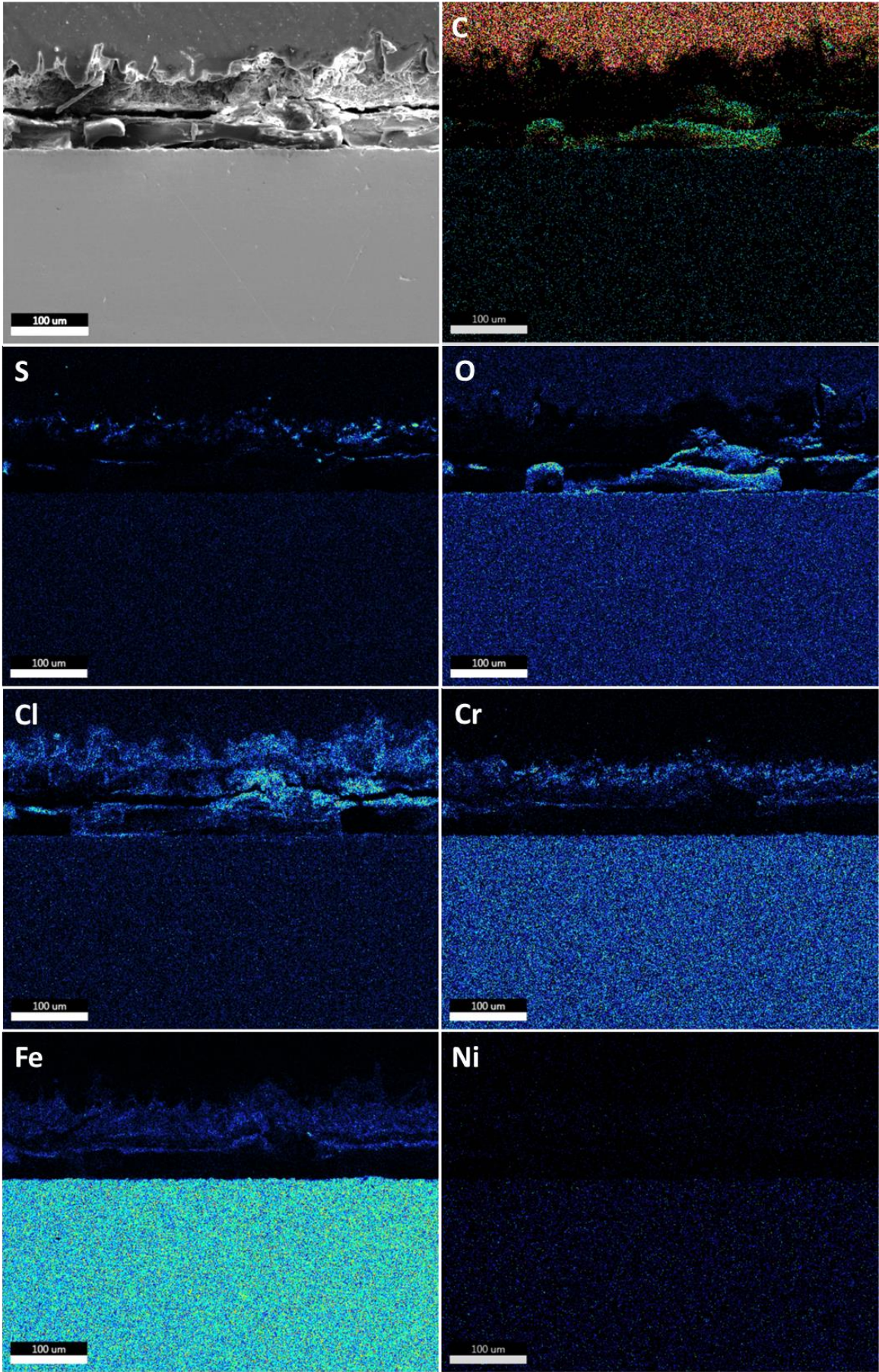


Figure 5.17 EDX mapping of a cross section of P9 steel at 480 °C after 240 h in the 50:50 mixture. The colour is connected with the concentration and increases from dark blue, light blue, green, yellow, orange to red. 580 °C

5.2.1.2 580 °C

Figures 5.18 and 5.19 show the typical appearance of the samples obtained after treatment at 580°C. The outer corrosion products on alloy 800HT are more loose compared to the ones after the experiments at 480 °C. The P9 steel has a black adherent corrosion layer on the whole surface, which did not spall as much as the one on alloy 800HT. However, compared to the experiments at 480 °C no significant differences, especially for P9 steel, were detected. The amount of resublimed FeCl_2 (Figure 5.20) is considerably higher compared with the experiment at 480 °C, in agreement with mass loss measurements (see 5.1)



Figure 5.18 Alloy 800HT after 240 h at 580 °C in the 50:50 gas atmosphere

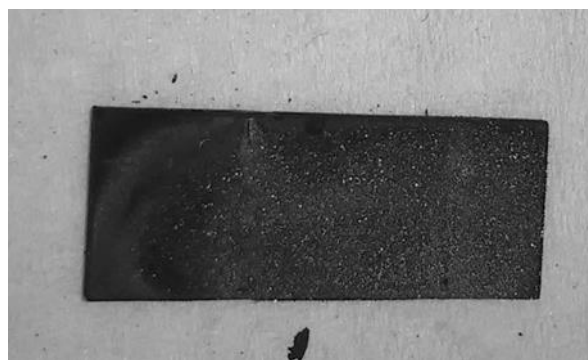


Figure 5.19 P9 steel after 240 h at 580 °C in the 50:50 gas atmosphere



Figure 5.20 Re-crystallized FeCl_2 in the silica glass pipe after 240 h at 580 °C

In Figure 5.21 the cross section of alloy 800HT after the 240 hours experiment is shown. There is a porous outer layer of corrosion products. Beneath this porous corrosion layer a gap of about 10 μm can be seen. This gap indicates a poor adhesion of the corrosion layer on the base material. After this gap, a region with material depletion follows. Furthermore the corrosion attack along the grain boundaries can be clearly seen.

Figure 5.23 shows the EDX mapping of alloy 800HT after 240 hours at 580 °C. The porous corrosion layer on top of the sample mainly consists of sulfur, chromium, iron and some oxygen, indicating the formation of a mixture of chromium and iron sulfides and small amounts of chromium oxide. The chromium oxide mainly exists under the sulfide layer, because of the already mentioned different permeability of sulfides and oxides for the gaseous molecules. Although Cr_2O_3 should be the thermodynamically stable phase at the given conditions, mainly sulfides define the corrosion layer. Beneath this sulfide layer the base material is mainly depleted in iron that was transformed by HCl to FeCl_2 and was eventually converted into iron sulfide or resublimed in the colder part of the silica glass pipe

after vaporisation. Compared to the experiments at 480 °C, only a very small amount of FeCl_2 remained in the corrosion layer. Chromium reacted at the metal-oxide-interface with HCl to CrCl_2 as well. Then it was transported towards the surface and reacted with the passing gas stream to chromium sulfides or oxides as soon as the partial pressure was adequate. Due to the material loss of iron and chromium in the base material, nickel remains as the primary component in this surface zone of the sample in agreement with the mapping that reveals an enrichment of nickel.

The oxygen mapping shows a high oxygen concentration on the left and right end. As already noted, this is caused by treatment with isopropanol during the grinding process and hence is not related with real corrosion products. The same applies for the high carbon content.

Figure 5.22 shows the cross section of P9 steel at 580 °C after 240 hours. The outer area of the corrosion scale consists of sulfides. This follows a voluminous layer of about 60 μm . The EDX mapping is shown in Figure 5.24. The sulfide layer on top of the corrosion products is mainly composed of iron and chromium with an increasing concentration of chromium sulfides on the inner side of the sulfide scale. The following voluminous layer is formed by a mixture of FeCl_2 , iron oxides and a small amount of Cr_2O_3 .

Furthermore, a constant material abrasion of the base material and no depletion of single materials like in alloy 800HT is observed. Again, the high carbon and oxygen concentrations in the zone of the base material do not represent real corrosion products and are assumed to be caused during the grinding procedure as noted above for the other samples.

Other areas with a high oxygen concentration are related to chromium and iron oxides. In contrast to thermodynamic calculations, also chromium sulfide exists and not only Cr_2O_3 . Again the sulfide layer is on the outer part of the corrosion products.

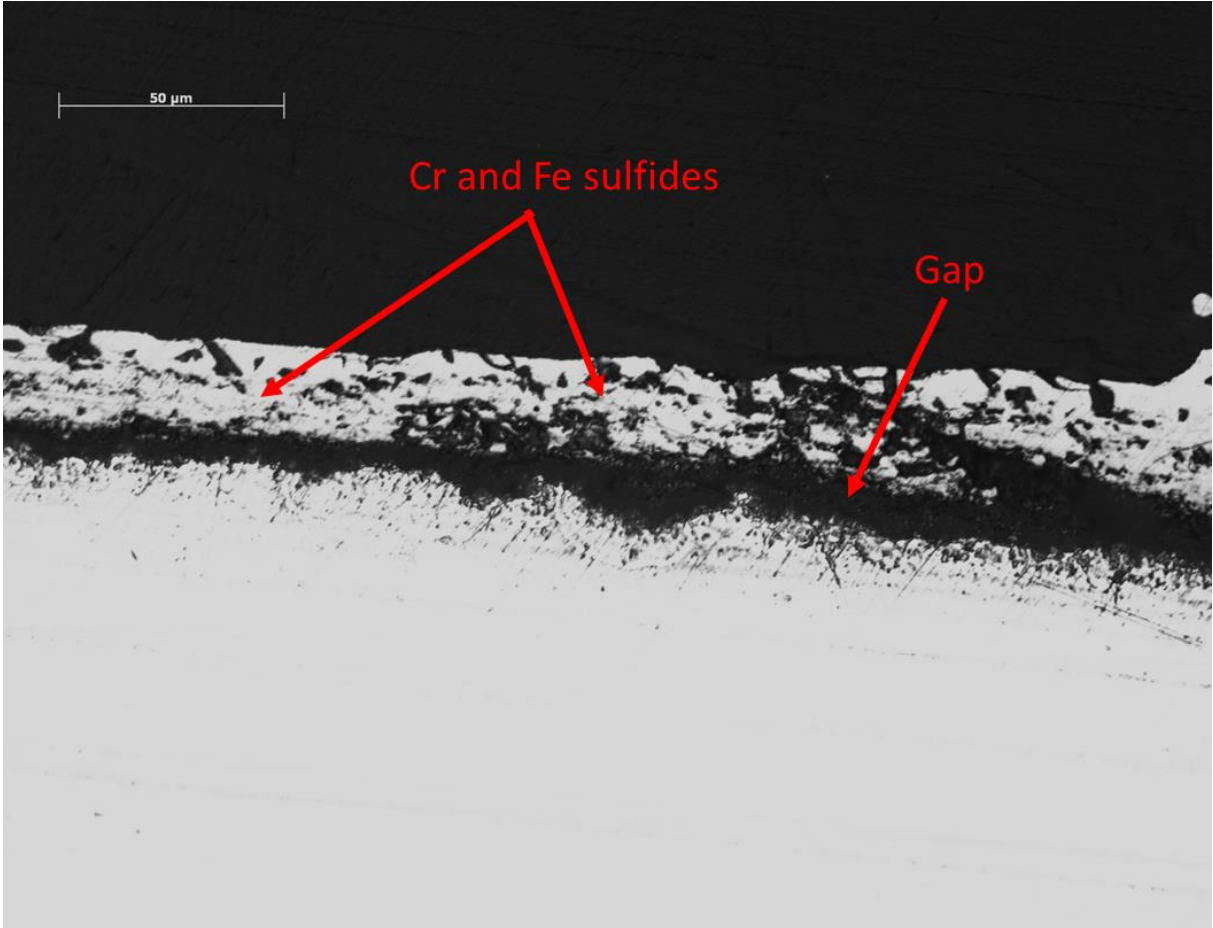


Figure 5.21 Cross section of alloy 800HT after 240 h at 580 °C

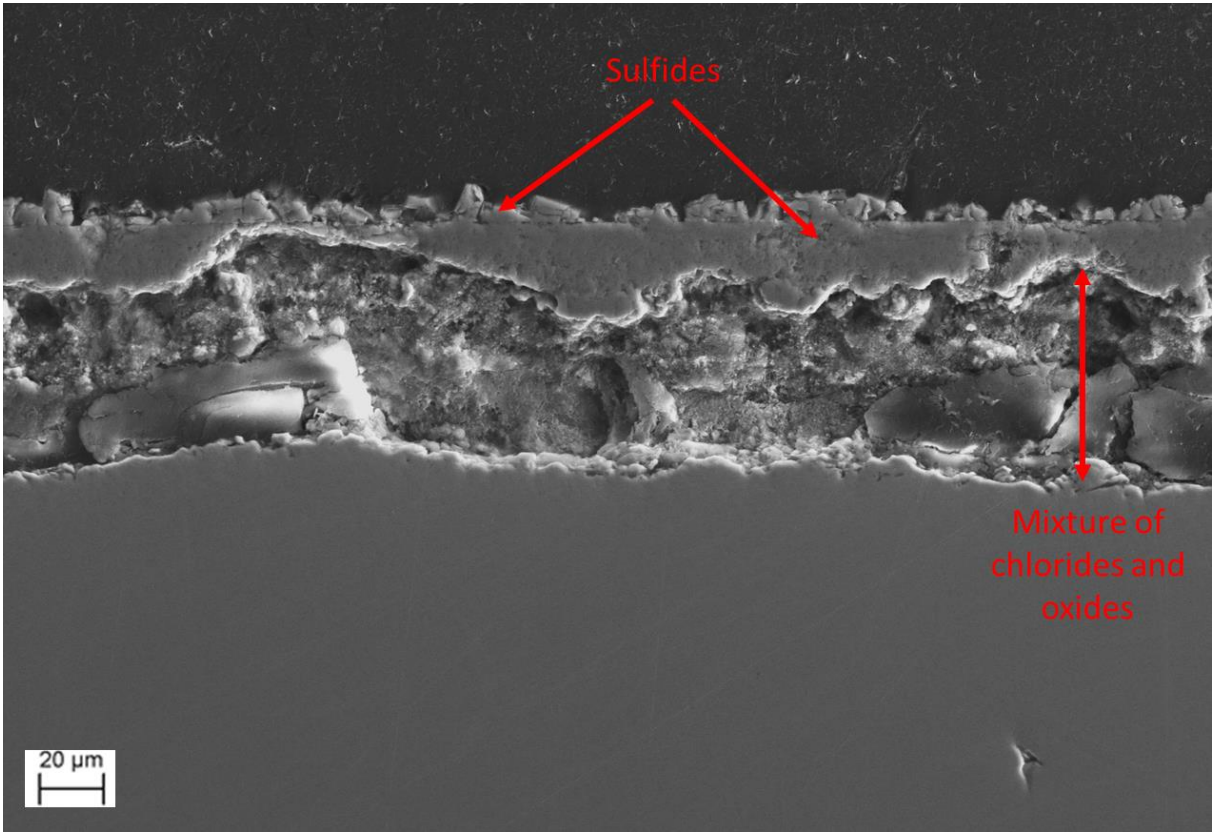


Figure 5.22 Cross section of P9 steel after 240 h at 580 °C

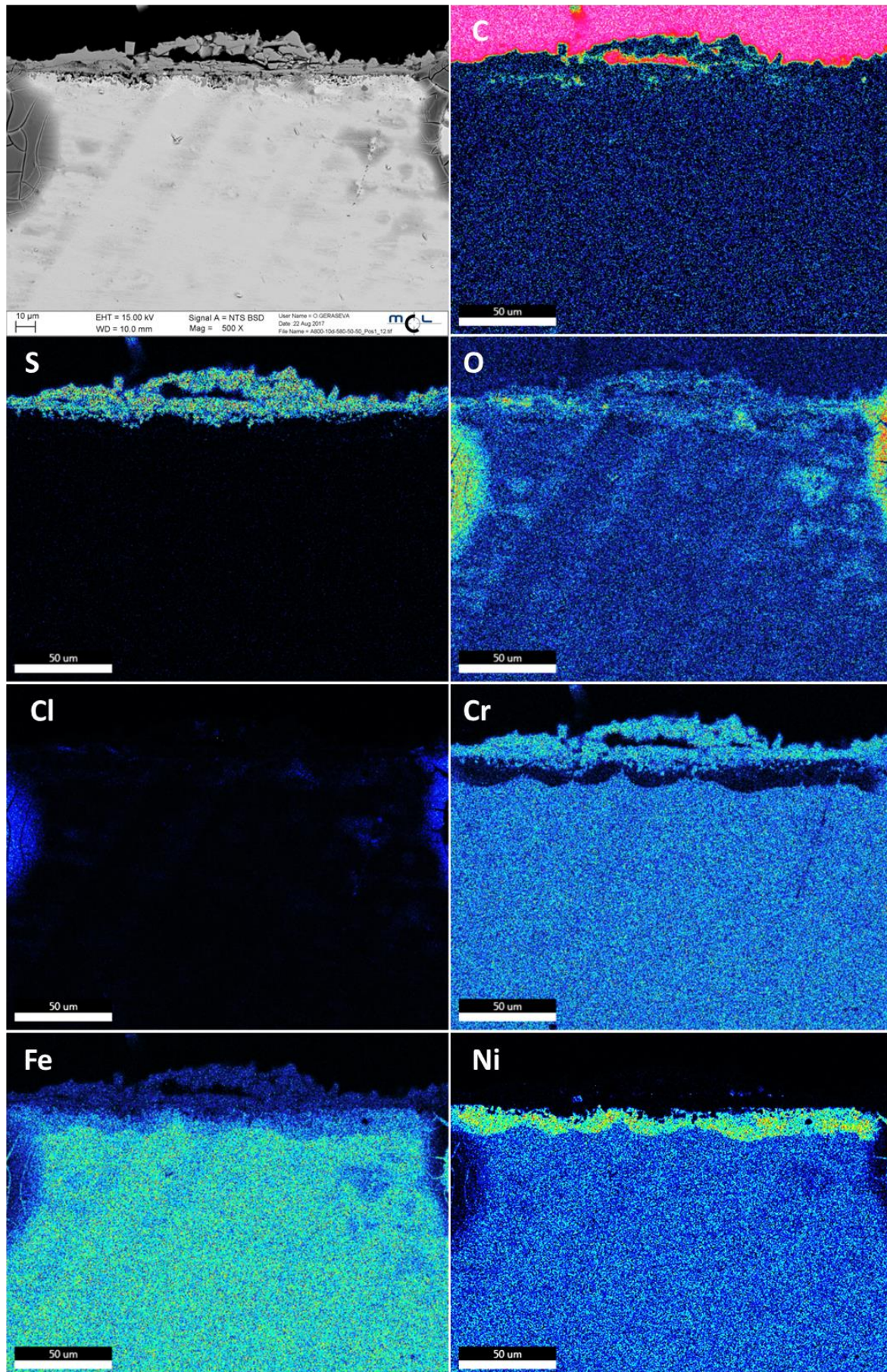


Figure 5.23 EDX mapping of a cross section of alloy 800HT at 580 °C after 240 h in the 50:50 mixture. The colour is connected with the concentration and increases from dark blue, light blue, green, yellow, orange to red.

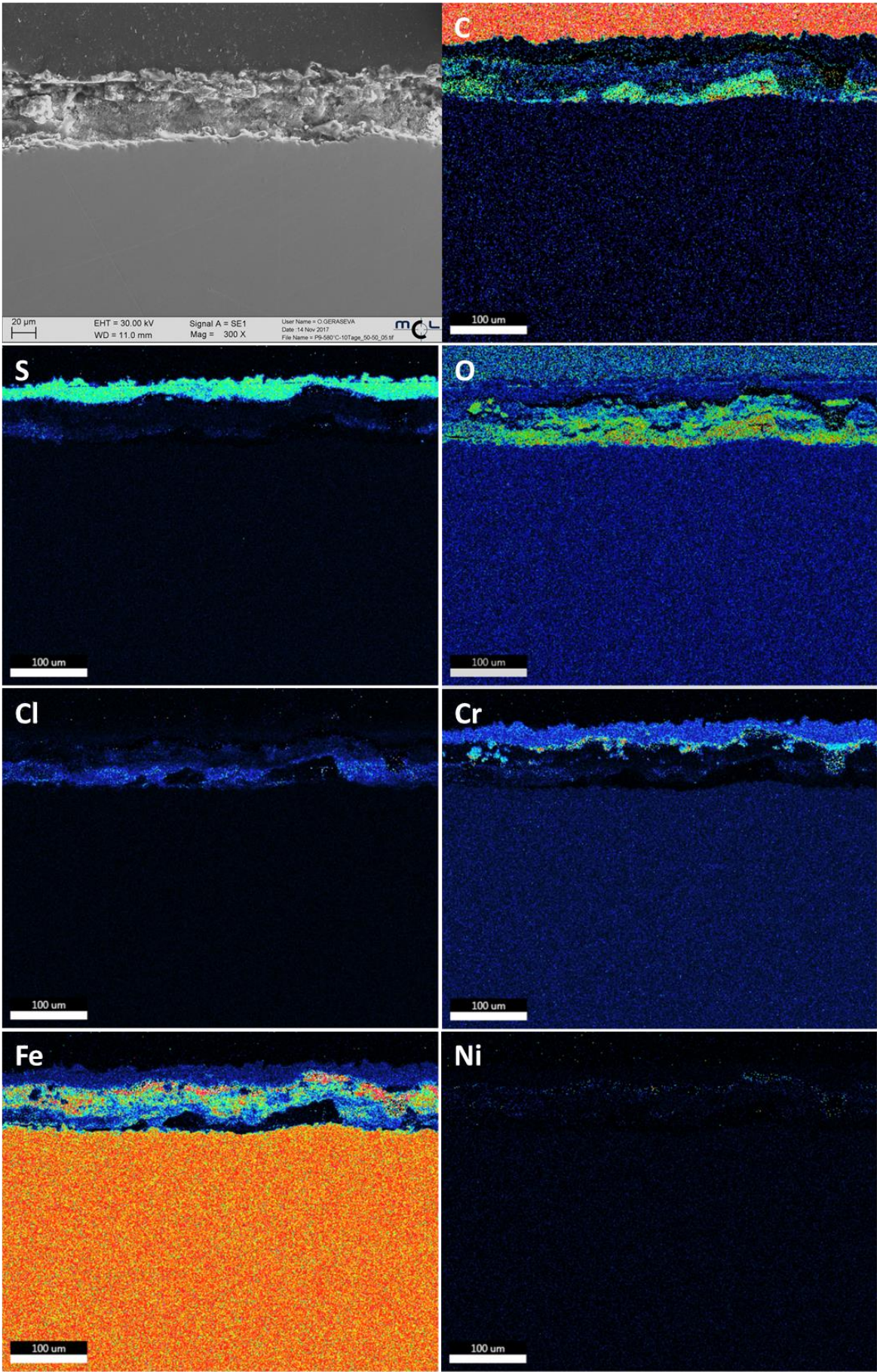


Figure 5.24 EDX mapping of a cross section of P9 steel at 580 °C after 240 h in the 50:50 mixture. The colour is connected with the concentration and increases from dark blue, light blue, green, yellow, orange to red.

5.2.1.3 680 °C

At the first sight the corrosion products on the samples obtained after the 680 °C experiments did not show differences compared to experiments with lower temperatures. As expected, the amount of FeCl_2 in the colder part of the silica glass tube was much higher (Figure 5.28). The appearance of the samples after 72 hours is shown in Figures 5.25 and 5.26. The corrosion layer on alloy 800HT was more adhere than the one after the 580 °C experiment although it spalled more than the one on P9 steel at the same experiment at 680 °C. The P9 steel had a thick corrosion layer over the whole surface which did not spall. On the upper end of the sample big crystals grew into the passing gas stream. Figure 5.27 shows a picture of the sample with the corrosion layer removed.



Figure 5.25 Alloy 800HT after 72 h at 680 °C in the 50:50 gas atmosphere



Figure 5.26 P9 steel after 72 h at 680 °C in the 50:50 gas atmosphere



Figure 5.27 P9 steel at 680 °C after 72 h in the 50:50 gas atmosphere, cleaned

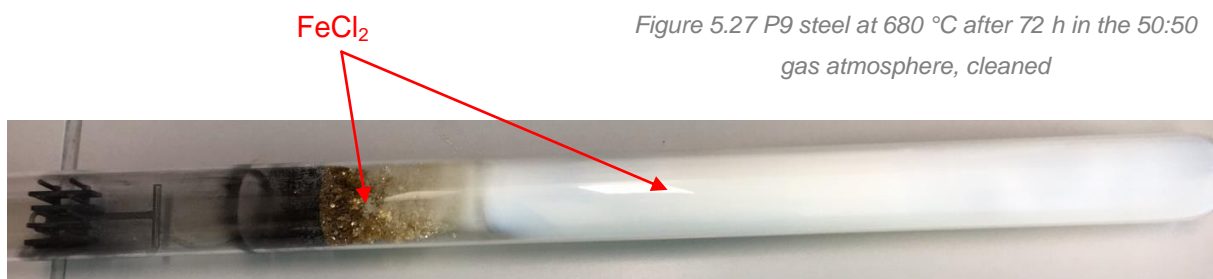


Figure 5.28 Re-crystallized FeCl_2 in the silica glass tube after 72 h at 680 °C

In the cross section of alloy 800HT after 240 hours at 680 °C (Figure 5.29) the corrosion layer is pictured. The outer layer consists of crystals which grew into the passing gas flow. Beneath this outer layer a thin scale was formed, followed by an area of chromium and iron depletion. Compared to the corrosion layer formed at 580 °C and 480 °C the one at 680 °C is less porous. This can be seen in the EDX mapping (Figure 5.31) where the carbon

concentration is pictured, because no carbon was detected inside the layer. The crystals on top of the sample mainly consisted of chromium sulfides. An XRD analysis revealed Cr_2S_3 and Cr_3S_4 as the main phases in this upper corrosion layer. Below this sulfide layer a nearly constant Cr_2O_3 layer was formed. In addition to this thin oxide scale, more Cr_2O_3 is located under this layer and reaches into the base material. The reason that the oxide grows under the sulfide can again be explained with the different permeability of the sulfides and oxides for the gaseous molecules. The diffusion through the sulfide layer is easier than through an oxide layer and therefore the oxide layer will be formed under the former. In the mapping, where the iron concentration is shown, severe iron depletion can be seen, which reaches about $20\mu\text{m}$ into the base material. However, nearly no iron was detected in the corrosion layer which leads to the conclusion that most of the iron will be converted into FeCl_2 and gets carried away with the passing gas flow and solidifies in the colder part of the silica glass tube. In addition to this iron depletion the formation of chromium chlorides and the subsequent formation of corresponding oxides and sulfides led to a depletion of chromium in the base material which reaches even deeper into the material than the one caused by iron. The remaining component is nickel, which barely reacts with the aggressive components in the gaseous atmosphere. This can be seen in the mapping where an enrichment of nickel is pictured. No nickel was detected in the corrosion layer, which leads to the conclusion that this metal gets more resistant against the sulfur attack, the higher the testing temperature is.

P9 steel has, compared to alloy 800HT, a much higher mass loss at $680\text{ }^\circ\text{C}$ and a thicker corrosion layer as shown in the cross section in Figure 5.30. It consists of a voluminous layer of about $200\text{ }\mu\text{m}$ with a comparable thin scale on top. The EDX mapping of P9 steel after 72 hours at $680\text{ }^\circ\text{C}$ is shown in Figure 5.32. The outer area is a porous Cr_2O_3 scale. According to the mapping this oxide layer is covered with a very thin sulfide layer, which consists of a mixture of iron and chromium sulfides. Again, this does not match with the phase stability diagram of chromium, where only Cr_2O_3 should exist. Although only very few reactive oxygen is available in the gas atmosphere, nearly all the formed chromium chloride was converted into Cr_2O_3 and into small amounts of chromium sulfide. This could be explained with the principle of supply and demand: The P9 steel only contains 9wt.% chromium, which leads to less chromium that can react with the HCl and therefore less CrCl_2 . The reduced amount of CrCl_2 results in less needed reactive oxygen to convert the chloride into Cr_2O_3 which is the thermodynamically more stable phase. Therefore the available oxygen is sufficient to convert nearly all the available chromium chloride and consequently only few amounts of sulfides are formed. Under this oxide scale is a very voluminous layer out of small amounts chromium oxide but mainly carbon. This carbon got into the pores of the voluminous construct during the mounting (see above).

Although the main component of the material is iron, only small amounts of iron in the corrosion layer are shown in the mapping because most of the iron will be carried away as FeCl_2 and crystallizes in the colder part of the silica glass tube. Only few FeCl_2 remains in the inner zone, right on the base material, where the oxygen partial pressure is low enough. Due to the high amount of FeCl_2 during the corrosion process of P9 steel some FeCl_2 are converted into iron sulfides and oxides. The corrosion attack occurs along the grain boundaries.

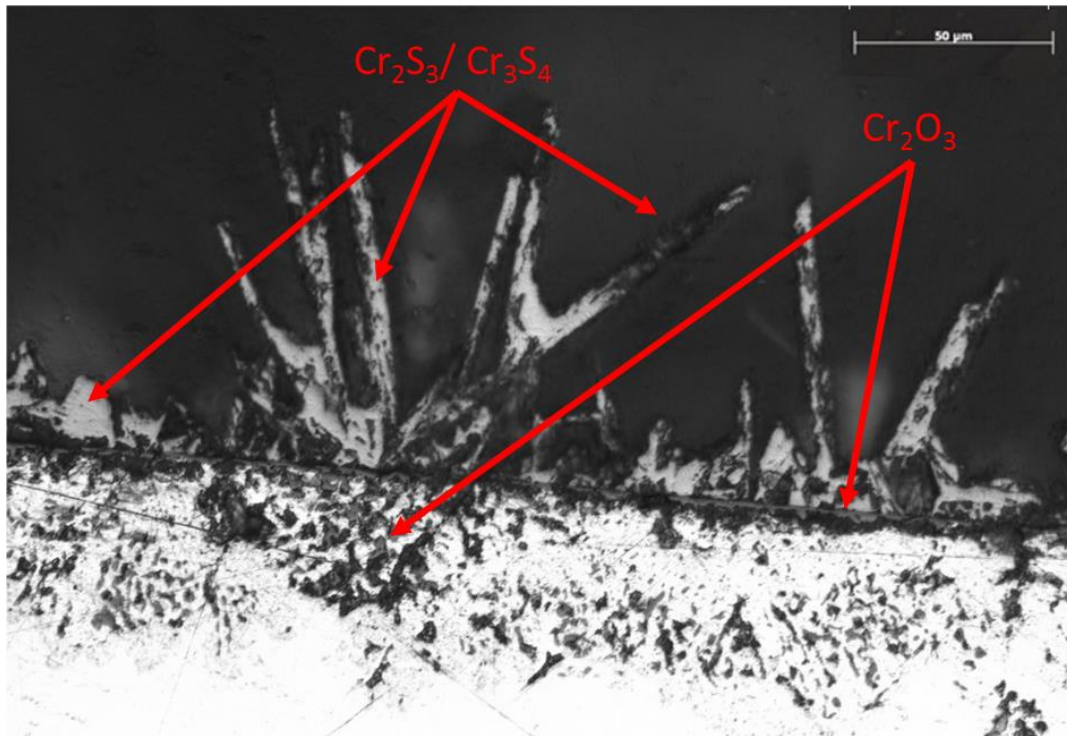


Figure 5.29 Cross section of alloy 800HT after 240 h at 680 °C

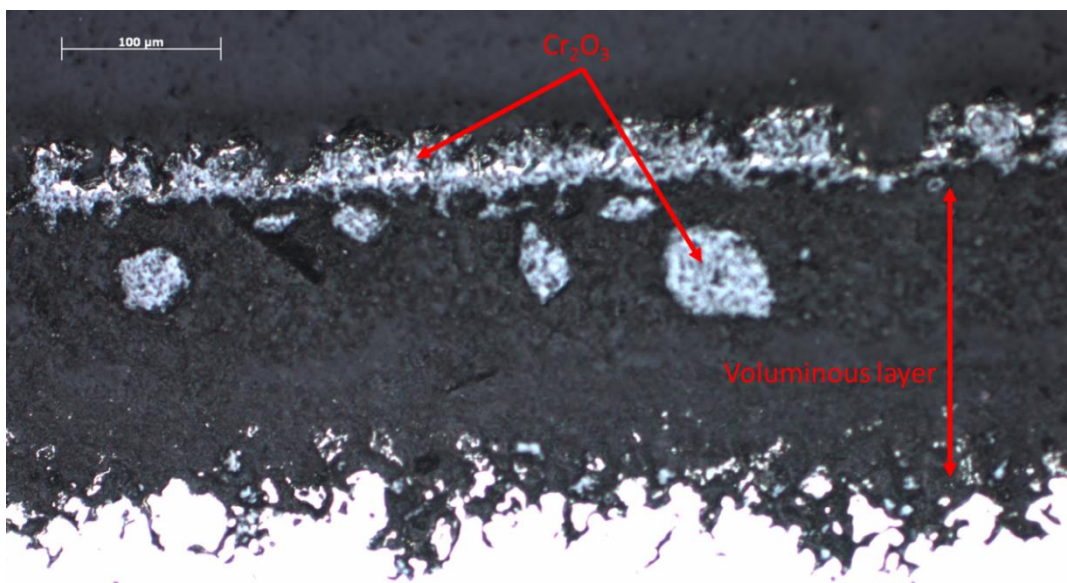


Figure 5.30 Cross section of P9 steel after 72 h at 680 °C

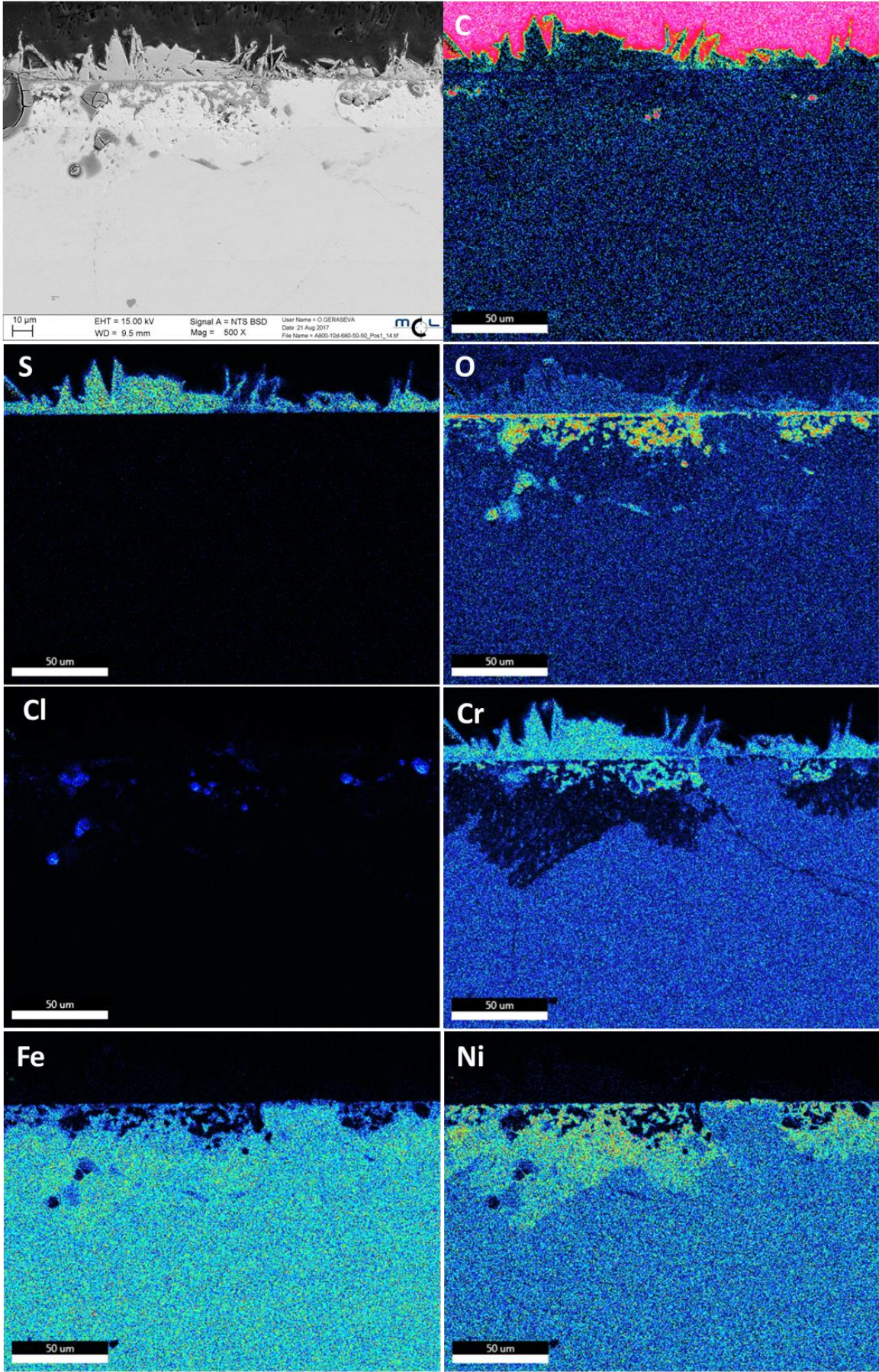


Figure 5.31 EDX mapping of a cross section of alloy 800HT at 680 °C after 240 h. The colour is connected with the concentration and increases from dark blue, light blue, green, yellow, orange to red.

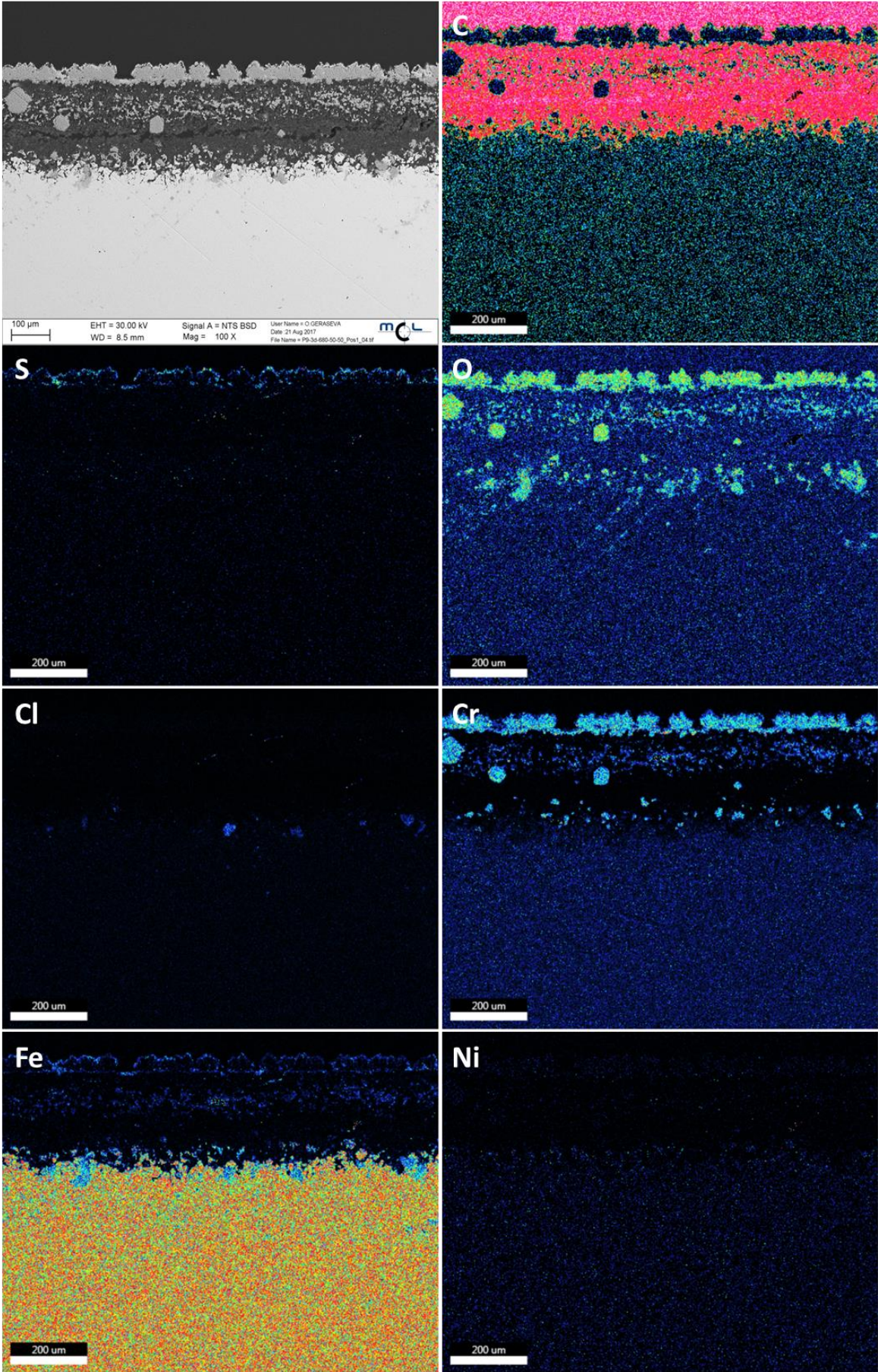


Figure 5.32 EDX mapping of a cross section of P9 steel at 680 °C after 72 h. The colour is connected with the concentration and increases from dark blue, light blue, green, yellow, orange to red.

5.2.2 Gas atmosphere without HCl

The appearance of the samples after the experiments in the H₂S atmosphere, where no HCl was present, showed significant differences compared to the appearances after the test runs with HCl. Again, the corrosion products will be discussed separately for each temperature.

5.2.2.1 480 °C

Figures 5.33 and 5.34 show the corrosion products after the experiments in the H₂S atmosphere at 480 °C. There are considerable differences between alloy 800HT and P9 steel. Alloy 800HT shows only a very thin corrosion layer whereas the P9 steel is surrounded by a thick sulfide layer. The missing part of the sulfide scale (Figure 5.34) broke away when the sample was removed from the sample holder, showing that the sulfide layer was not adherent. The corrosion layer was easy to remove with a wired brush and the 5% HCl solution in the ultrasonic bath. The same applies for the cleaning process of alloy 800HT.



Figure 5.33 Alloy 800HT after 240 h at 480 °C in the 100:0 gas atmosphere

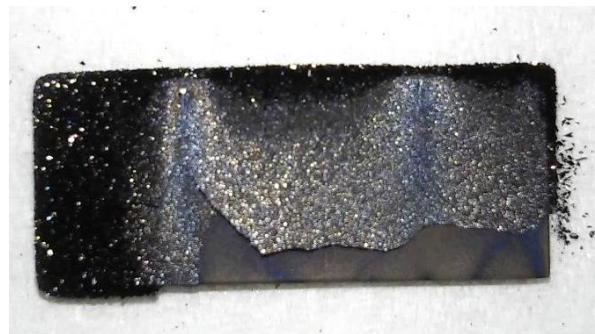


Figure 5.34 P9 steel after 240 h at 480 °C in the 100:0 gas atmosphere

In Figure 5.37 the EDX mapping of alloy 800HT after 240 hours at 480 °C is given. The cross section of alloy 800HT (Figure 5.35) shows a thin corrosion layer with numerous hollow spaces. Those layers mainly consist of iron and nickel sulfides with a thin iron oxide layer below. This sulfide formation leads to an iron and nickel depletion in the base material, and only chromium remains. This forms a Cr₂O₃ scale on the outer side of the material. The depletion does not reach far into the material.

In case of P9 steel the corrosion layer has a completely different appearance, which shows the cross section depicted in Figure 5.36. The outer area is formed by large crystals of about 400 µm which grew into the passing gas stream. Beneath them an area with smaller crystals had formed. This is probably the reason for the poor adherence on the base material. According to the EDX mapping of P9 steel (Figure 5.38) the crystals consist of iron sulfides. As known from the previous mapping of alloy 800HT chromium nearly does not react with the H₂S in the atmosphere at a temperature of 480 °C. Therefore chromium

remains in the base material, which leads to an enrichment that can be seen in the mapping. However, due to the high amount of sulfur detected in the base material, a small amount of chromium also forms chromium sulfide. Oxygen is located in the base material, as shown by chromium oxide formation. The constant formation of iron sulfides leads to a material depletion in the base material. This, however, occurs along a constant line.

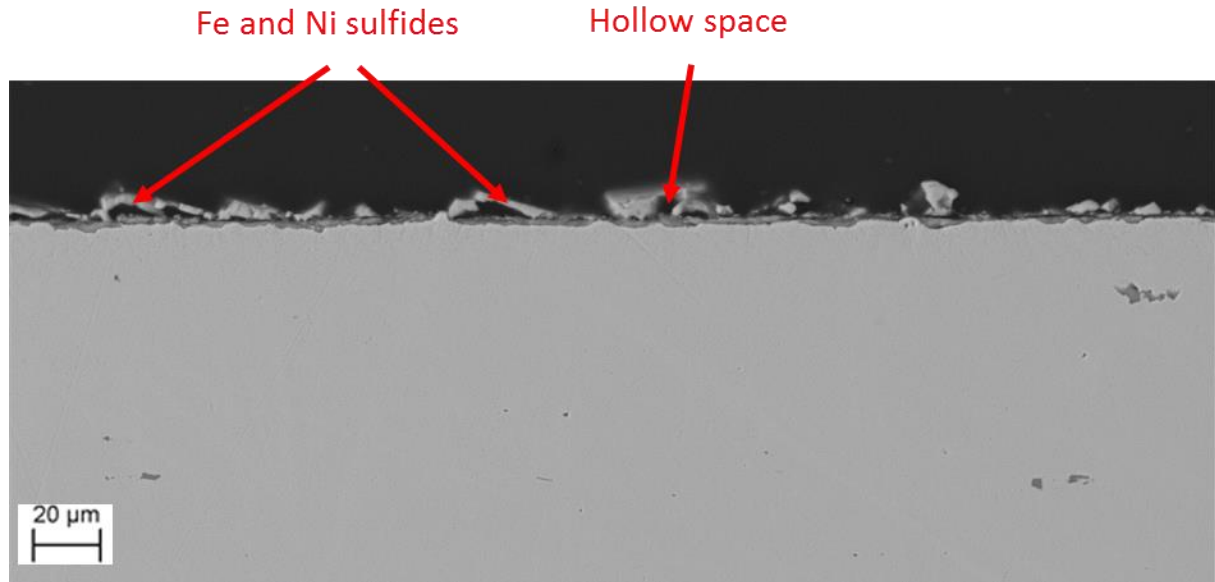


Figure 5.35 Cross section of alloy 800HT after 240 h at 480 °C

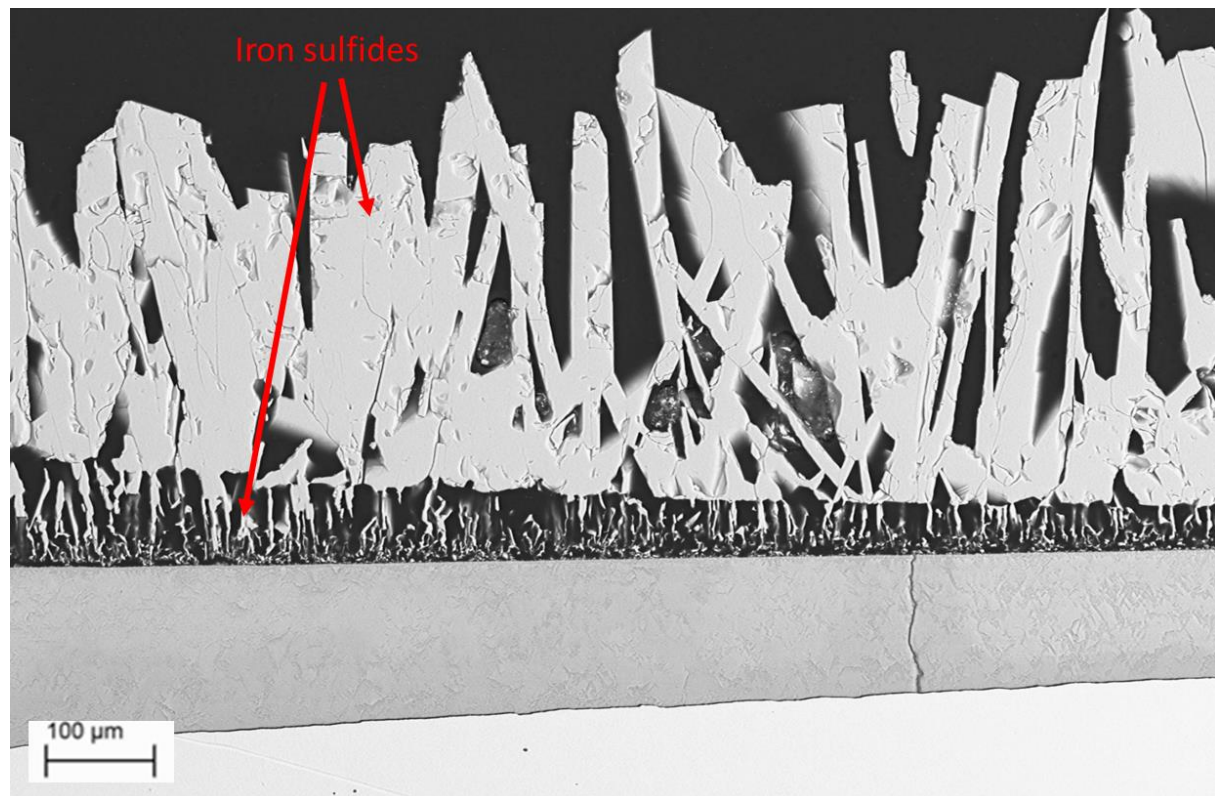


Figure 5.36 Cross section of P9 steel after 240 h at 480 °C

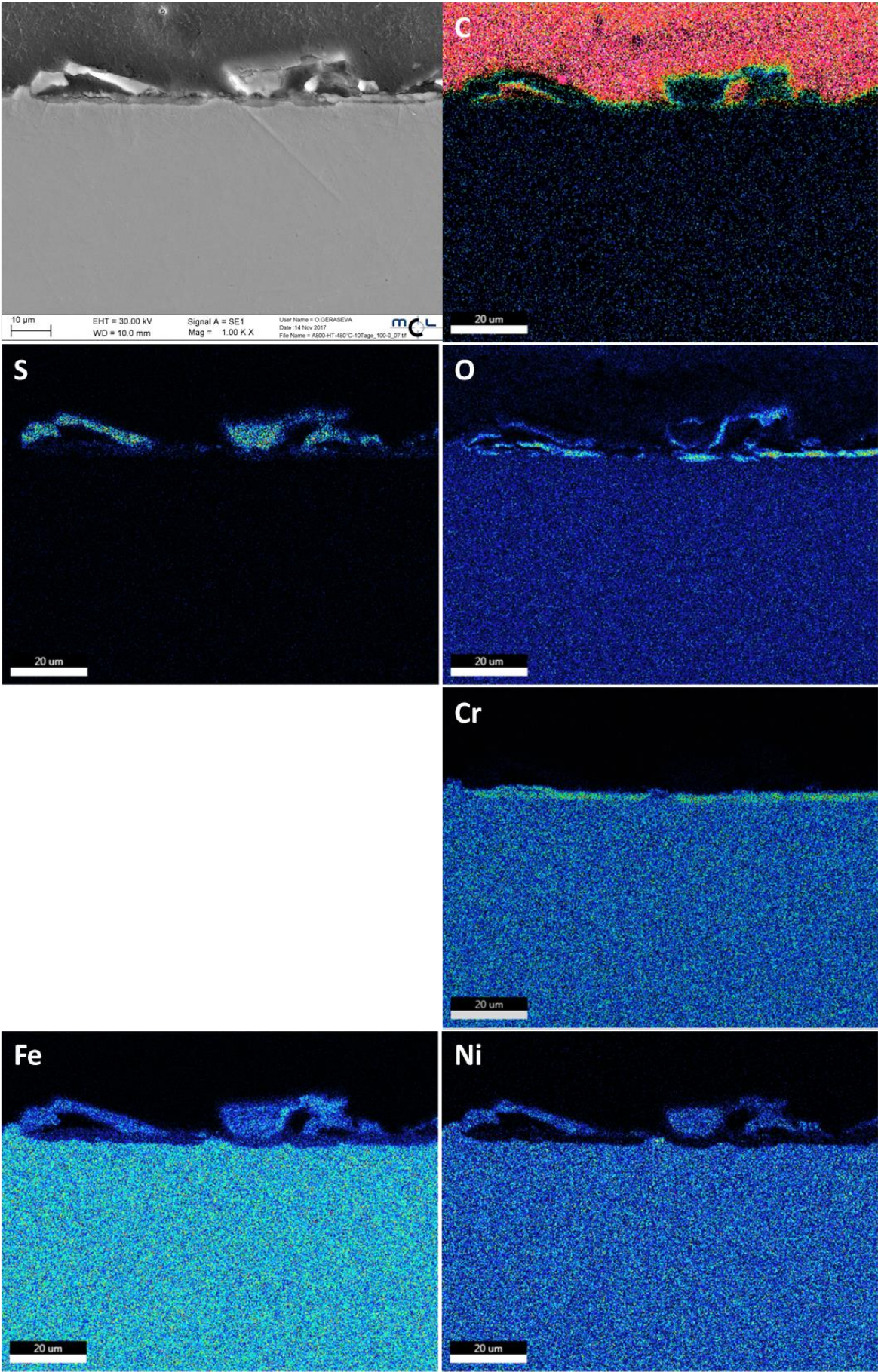


Figure 5.37 EDX mapping of a cross section of alloy 800HT at 480 °C after 240 h in the 100:0 mixture. The colour is connected with the concentration and increases from dark blue, light blue, green, yellow, orange to red.

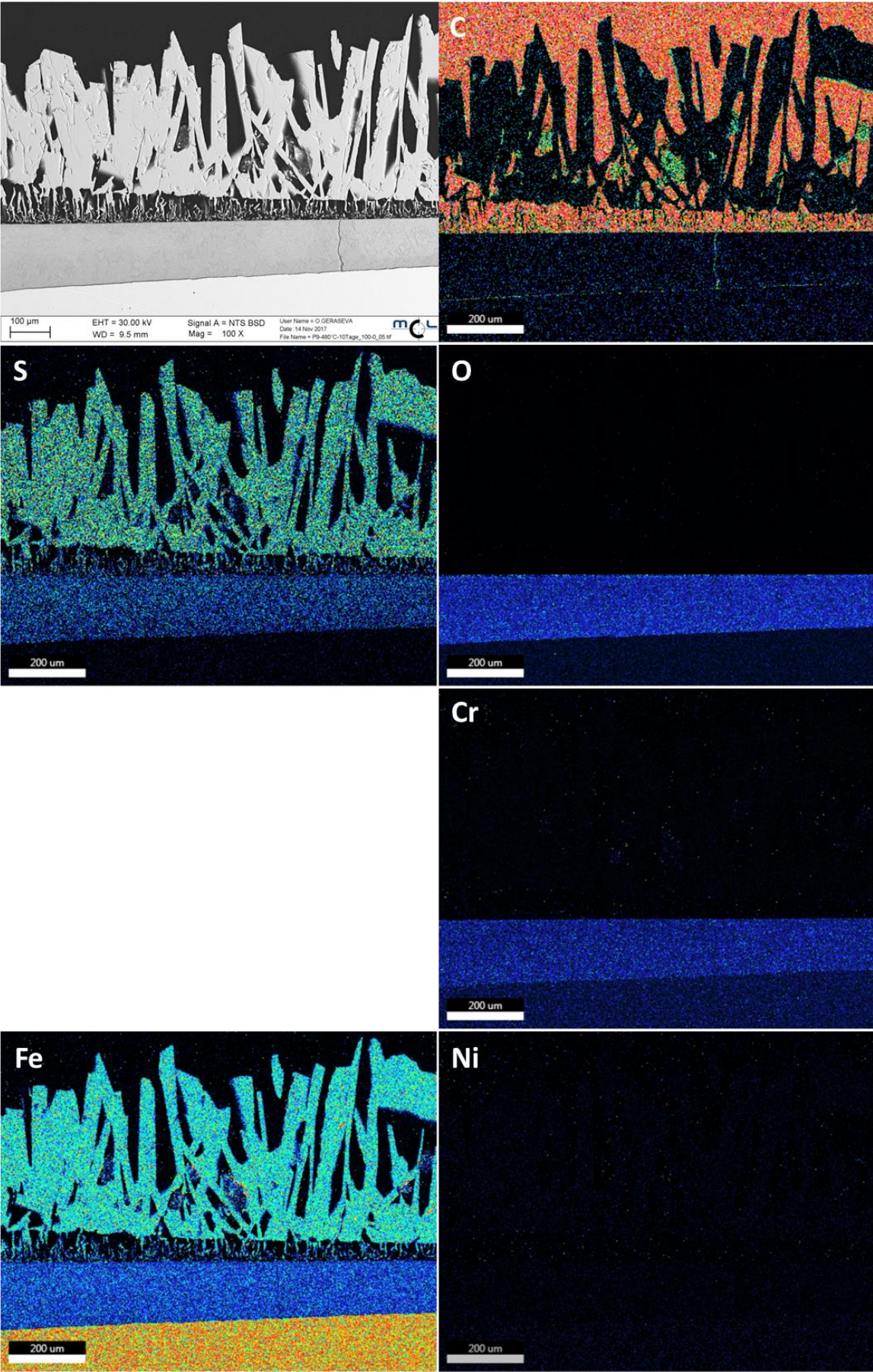


Figure 5.38 EDX mapping of a cross section of P9 steel at 480 °C after 240 h in the 100:0 mixture. The colour is connected with the concentration and increases from dark blue, light blue, green, yellow, orange to red.

5.2.2.2 680 °C

At 680 °C the corrosion products show complete different appearances, compared to 480 °C. The samples are pictured in Figures 5.39 and 5.40. Alloy 800HT is characterized by a black corrosion layer and on the top by small sulfide crystals. The P9 steel had an ancillary black corrosion layer covering the whole surface, but additionally large sulfide crystals grow on a restricted area of the sample. Both specimens had to be cleaned with two subsequent steps in the ultrasonic bath using at 5% HCl solution to remove all corrosion products because they were very adhering to the sample surface. The most severe corrosion occurred at the area where the large sulfide crystals were located (Figure 5.41). The surface of the other part of the sample showed a comparatively low damage by corrosion.

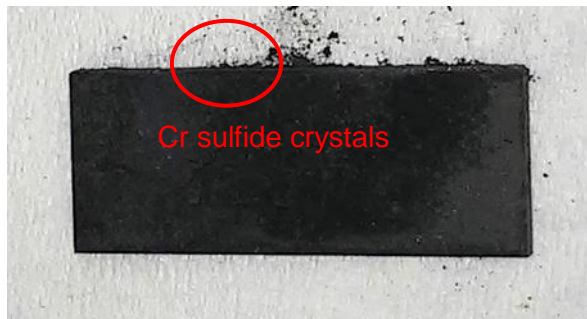


Figure 5.39 Alloy 800HT after 240 h at 680 °C in the 100:0 gas atmosphere

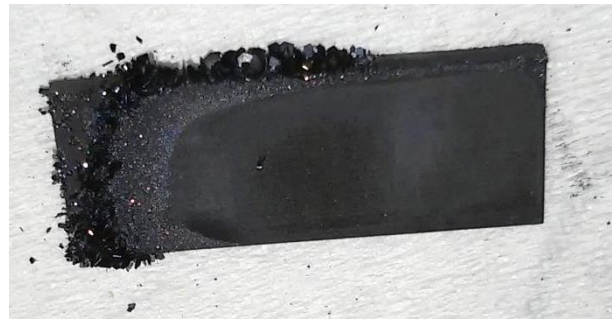


Figure 5.40 P9 steel after 240 h at 680 °C in the 100:0 gas atmosphere



Figure 5.41 P9 steel after 240 h at 680 °C in the 100:0 gas atmosphere, cleaned

The cross section of alloy 800HT is shown in Figure 5.42. Crystals of different sizes grew on top of the corrosion layer into the passing gas stream. Beneath those crystals a spalled layer is located. According to the EDX mapping (Figure 5.44), the sulfide crystals on top of the layer mainly consist of chromium sulfide. Beneath this sulfide layer a very thin Cr_2O_3 layer is located. The formation of chromium sulfides and oxides leads to a chromium depletion in the material, which reaches about 10 μm into the sample.

Nearly no iron is detected in the corrosion layer. The same applies for nickel. Both components remain in the base material which can be seen in an enrichment of iron and nickel in the mapping.

The cross section of P9 steel sample is shown in Figure 5.43. The outer corrosion layer is about 40 μm thick. On some areas large crystals grew into the passing gas flow. Beneath this layer a gap with small amounts of sulfides is located. This is followed by a very porous sulfide scale within the sample. According to the EDX mapping of P9 steel after 240 hours at 680 $^{\circ}\text{C}$ the outer layer with the big crystals mainly consist of iron sulfides with a very small amount of chromium (Figure 5.45). The surface area of the sulfides is surrounded by a very thin iron oxide scale. The porous structure inside the sample is formed by a mixture of iron and chromium sulfides and oxides. At the interface of the base material and the corrosion products the oxide concentration is the highest.

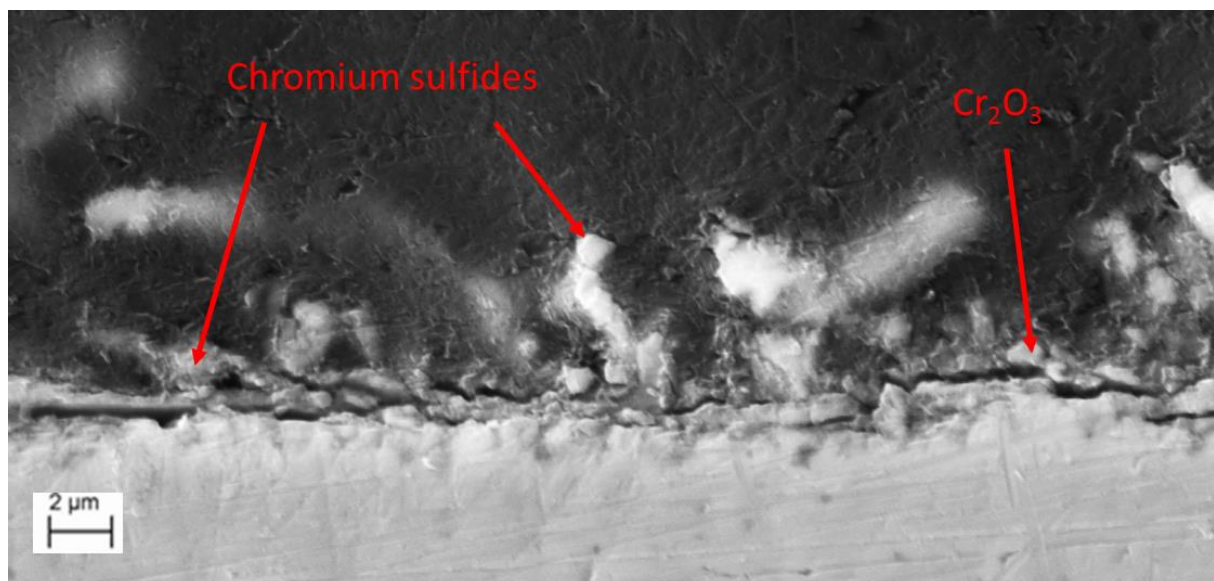


Figure 5.42 Cross section of alloy 800HT after 240 h at 680 $^{\circ}\text{C}$ in the 100:0 mixture

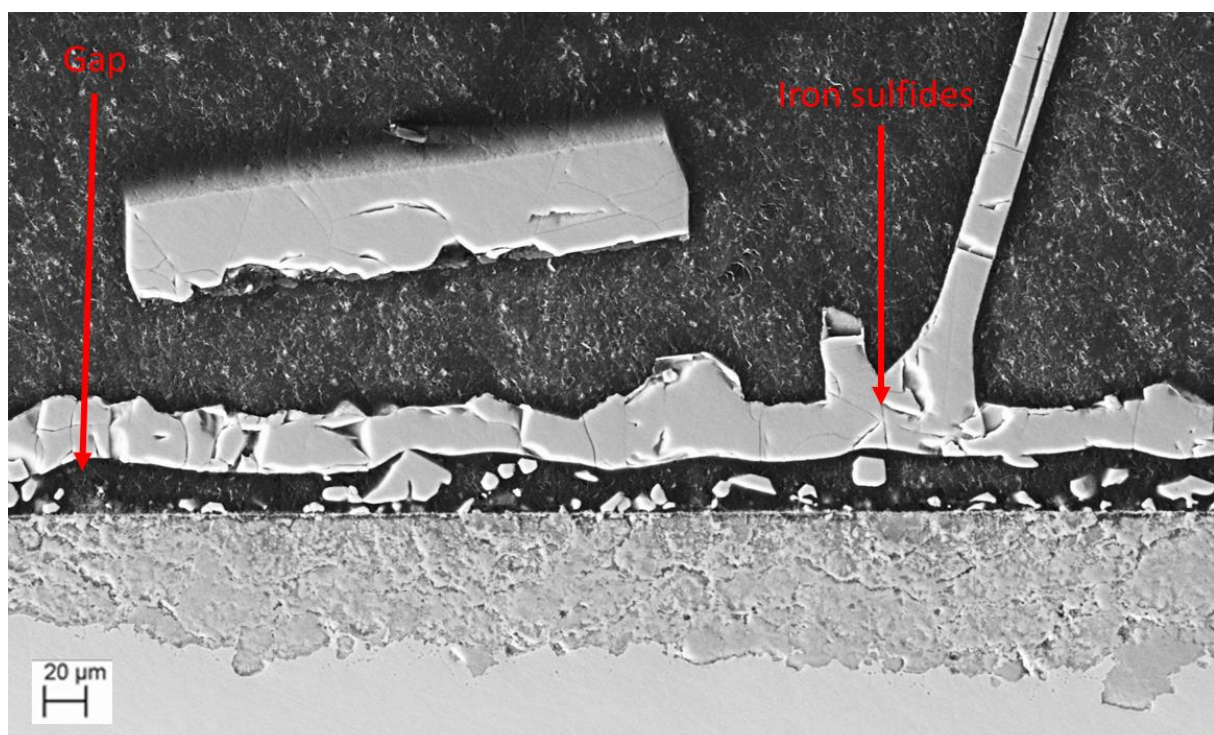


Figure 5.43 Cross section of P9 steel after 240 h at 680 $^{\circ}\text{C}$ in the 100:0 mixture

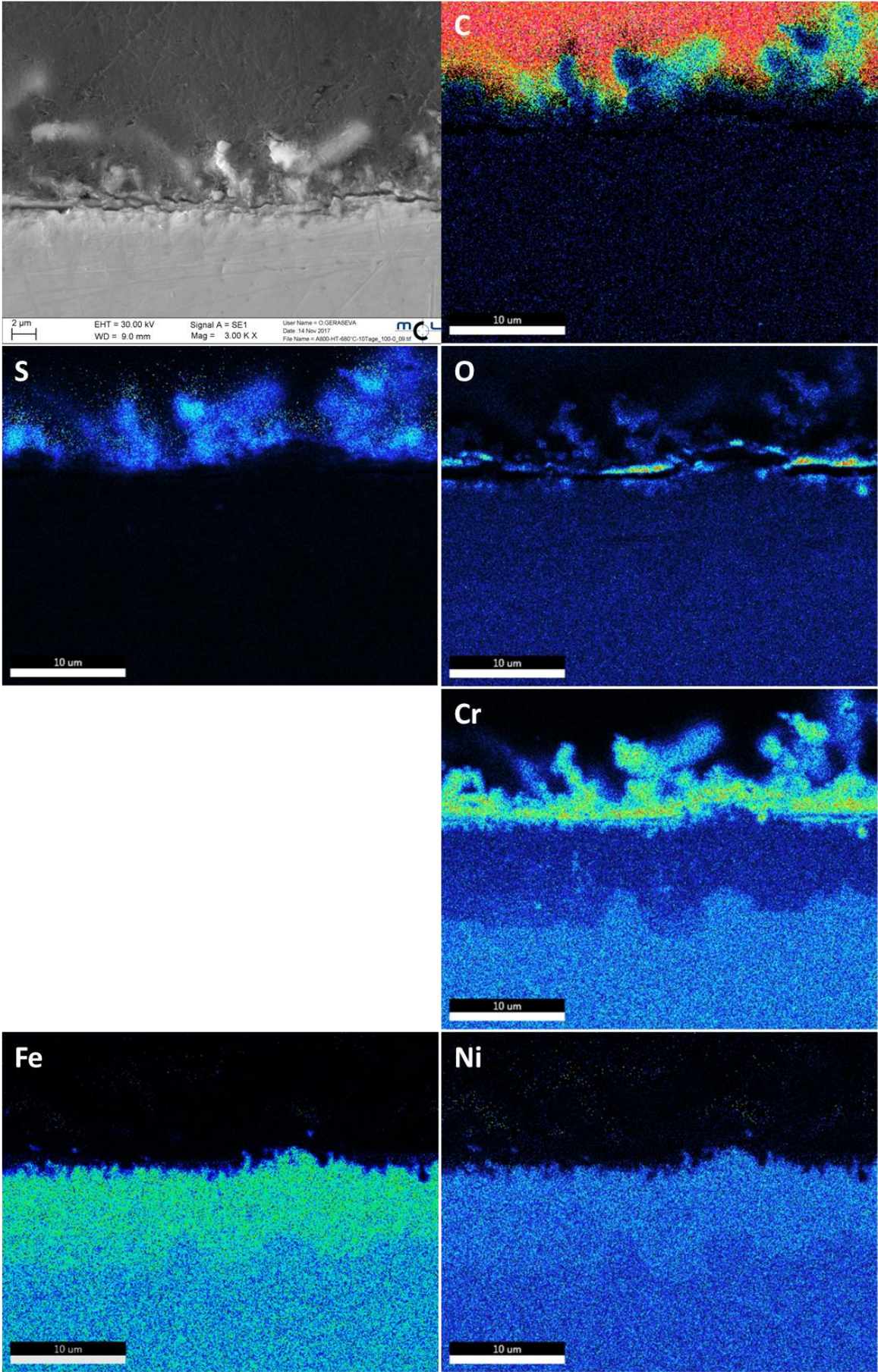


Figure 5.44 EDX mapping of a cross section of alloy 800HT at 680 °C after 240 h in the 100:0 mixture. The colour is connected with the concentration and increases from dark blue, light blue, green, yellow, orange to red..

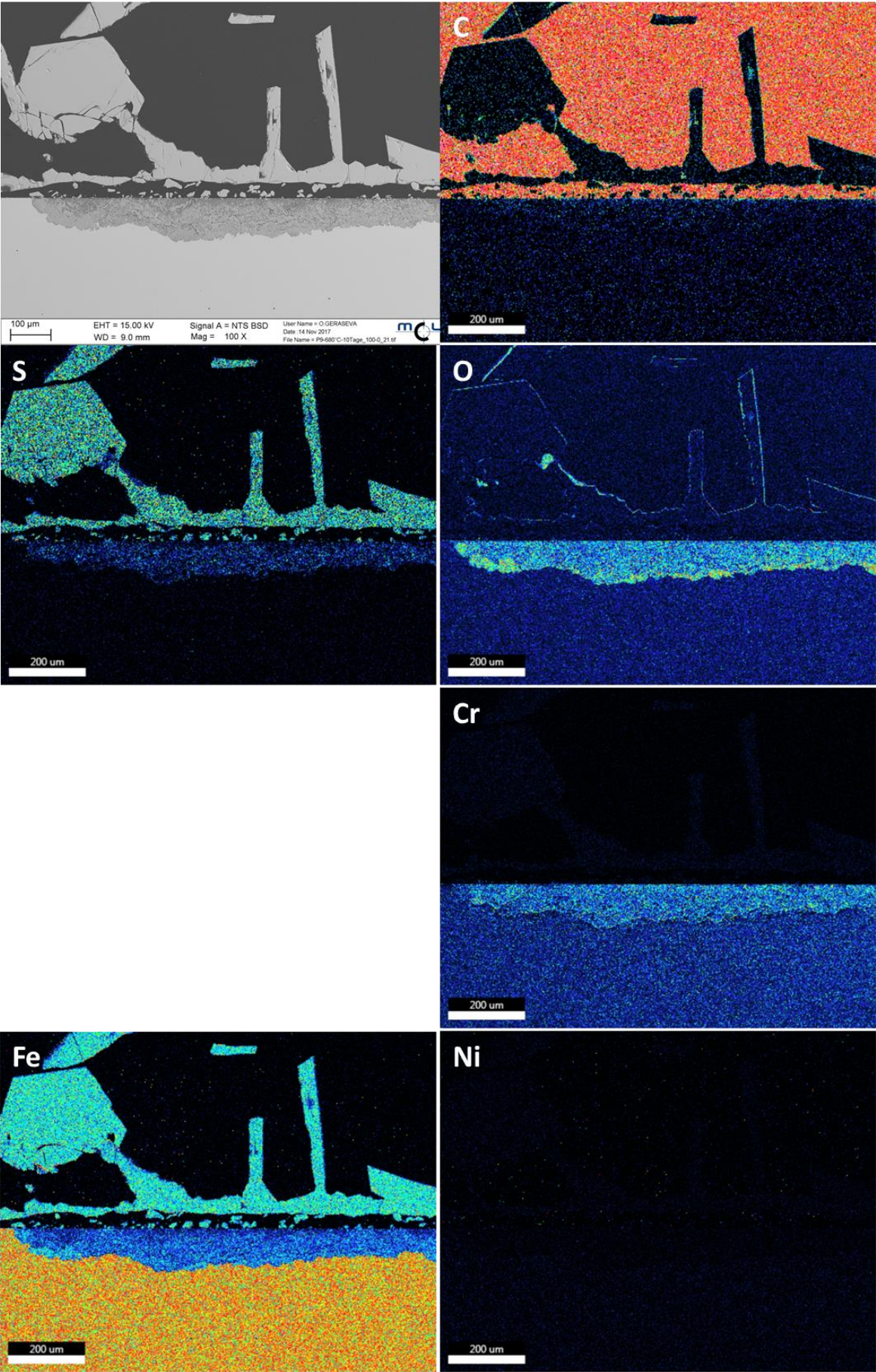


Figure 5.45 EDX mapping of a cross section of P9 steel at 680 °C after 240 h in the 100:0 mixture. The colour is connected with the concentration and increases from dark blue, light blue, green, yellow, orange to red.

5.3 Microstructure analysis

5.3.1 Gas atmosphere with HCl

To get more information about the effect of the corrosion on the microstructure of the materials, selected samples (cleaned from corrosion products) were hot mounted, polished and etched. Figure 5.46 shows the etched samples of alloy 800HT [(a), (b), (c)] and P9 steel [(d), (e), (f)] after the experiments at different temperatures. All samples were treated for 72 hours. The etching periods are listed in Table 5.1.

The first P9 steel sample was etched with Beraha-II, which led to too many overetched areas. Therefore the other P9 steel samples were etched with less aggressive Beraha-I. Nevertheless, these samples were also overetched. It was nearly impossible to prevent this over etching because of the corrosion pits in which the etchant moved into.

In case of P9 steel a ferritic structure is present. The outer areas suffered under severe corrosion attack, leading to more pores in which the etchant can move into and continue the etching. This leads to an overetching which is expressed by more intensive colours. This coloured area intensifies with the increase of the temperature and matches with the mass loss measurements, for which an increase of the mass loss is observed with rising temperature.

Figure 5.46 (f) depicts that the outer area of the sample is stronger etched compared to the specimens treated under lower testing temperatures. This is most likely a consequence of the severe chlorine attack and the resulting large amount of holes in the surface area of the sample, in which the etchant was able to move into. Additionally, the corrosive attack along the grain boundaries is visible in this Figure.

The etched samples of alloy 800HT have very different appearances than the P9 steel specimens. The microstructure has now an austenitic structure and no coloured outer areas are visible. Only a few zones indicate a deeper corrosion attack, as marked in Figure 5.46 (a). Here the etchant was able to migrate into, caused by corrosion pits too. The small amount of coloured areas agrees with previous mass loss measurements of alloy 800HT. The mass loss was quite small and did not increase markedly with rising temperature.

Table 5.1 Etching periods for the samples in the gas atmosphere with HCl

Alloy 800HT			P9 steel		
a)	Beraha-II	60s	d)	Beraha-I	60s
b)	Beraha-II	60s	e)	Beraha-I	60s
c)	Beraha-II	60s	f)	Beraha-II	40s

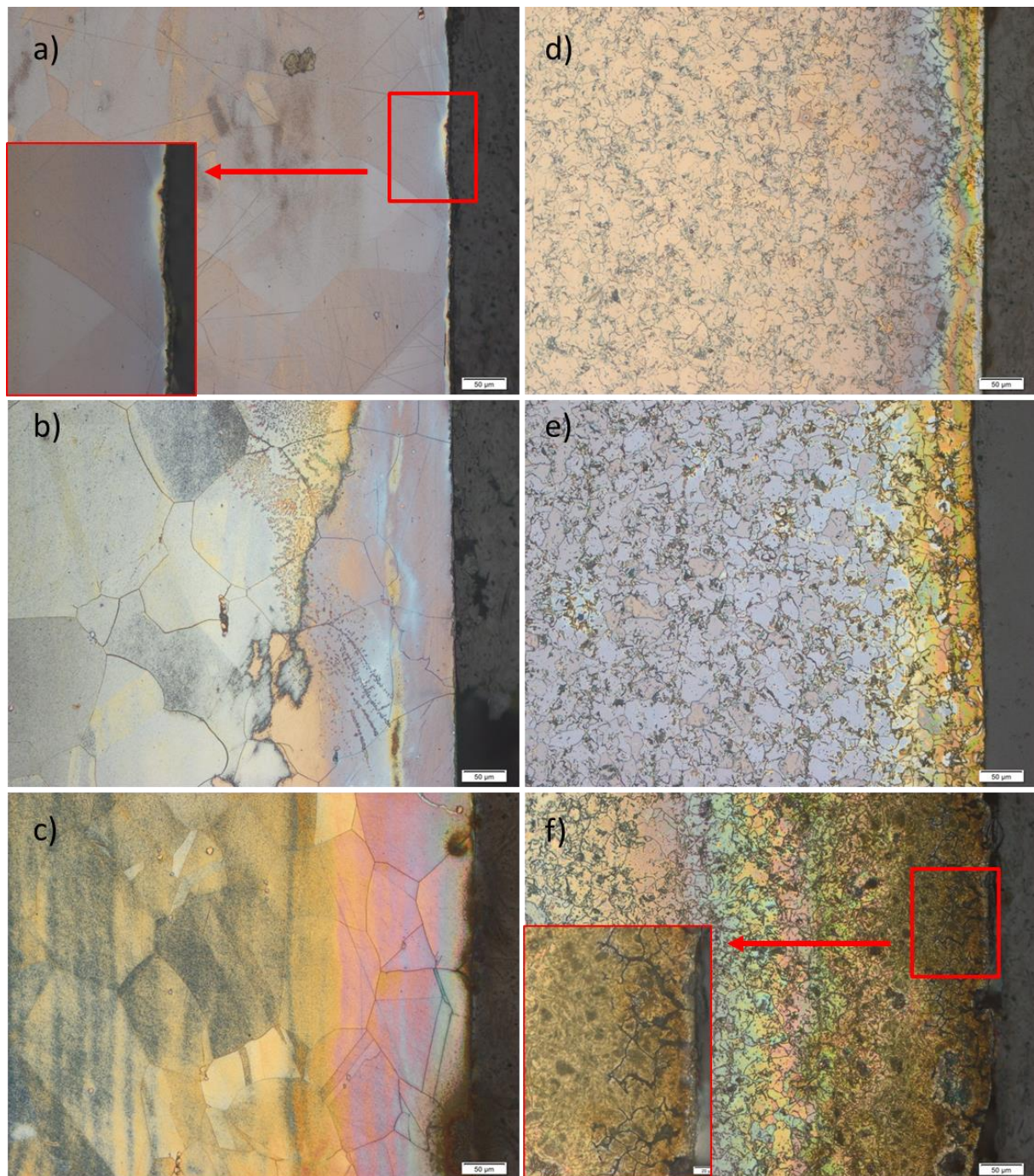


Figure 5.46 Light microscopy pictures (magnification 200x) of the cleaned samples after the experiments in the 50:50 mixture: Alloy 800HT: (a) 480 °C; (b) 580 °C; (c) 680 °C // P9 steel (d) 480 °C; (e) 580 °C; (f) 680 °C

5.3.2 Gas atmosphere without HCl

In Figure 5.47 the etched samples of alloy 800HT and P9 steel after 240 hours in the testing atmosphere without HCl are pictured. Again, the etching was performed both with Beraha-I and -II. The etching periods for each sample are listed in Table 5.2.

The corrosion in the sulfidising atmosphere shows a more constant surface abrasion compared to the chlorine-induced corrosion. At 480 °C alloy 800HT showed a very thin coloured area, which indicates no severe corrosion. H₂S only attacked the surface of the

sample and did not penetrate into the material. With rising temperature an increase of this attacked zone is visible.

P9 steel had a similar appearance after the experiment in the gas atmosphere without HCl at 480 °C, compared to the one with HCl at the same temperature. The surface zone was slightly overetched as well, which indicates the corrosive attack. At 680 °C the sample showed a different appearance compared to the experiments in the HCl-containing atmosphere. The corrosive attack in the sulfidising atmosphere does not occur along the grain boundaries and is not as severe as in the HCl-containing testing gas.

Table 5.2 Etching periods for the samples in the gas atmosphere without HCl

Alloy 800HT			P9 steel		
a)	Beraha-II	50s	c)	Beraha-I	60s
b)	Beraha-II	40s	d)	Beraha-I	70s

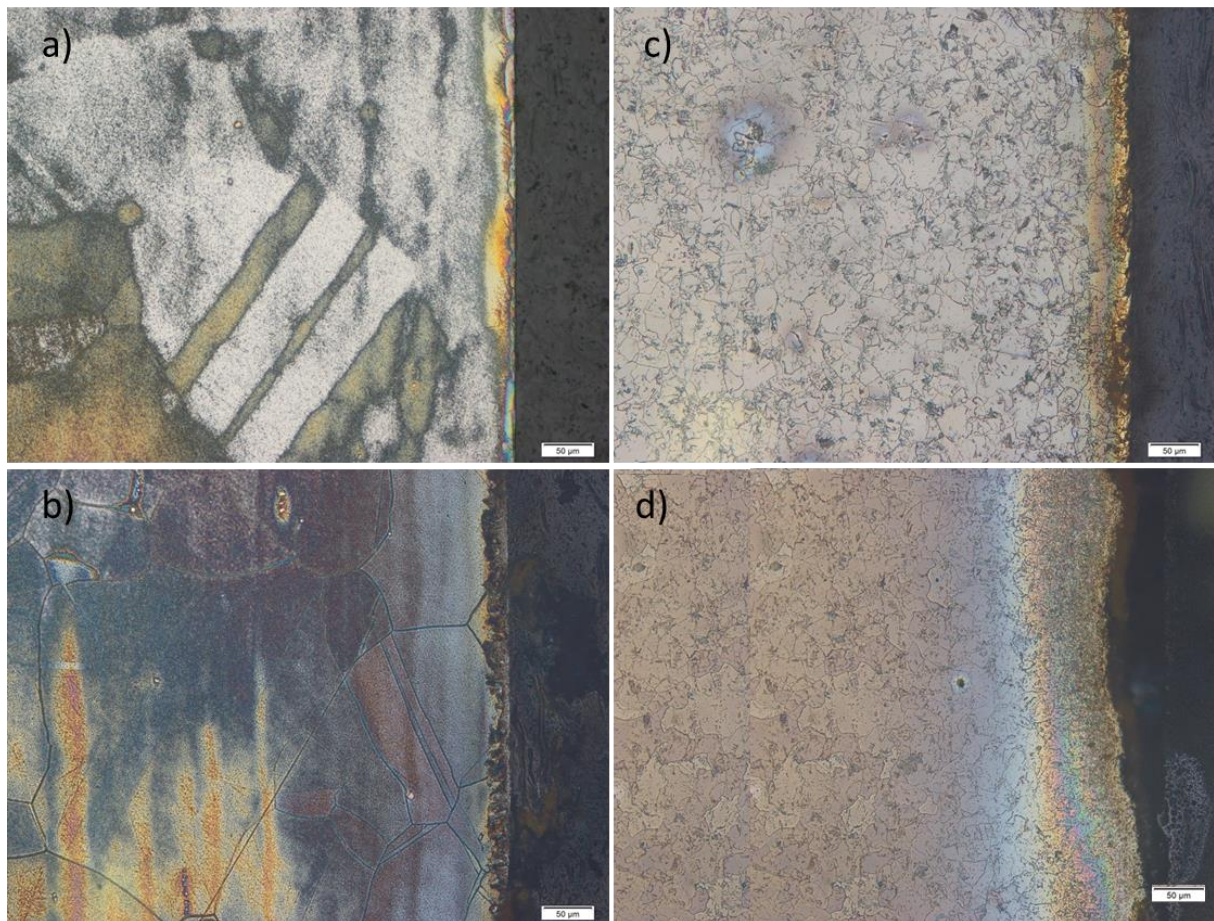


Figure 5.47 Light microscopy pictures (magnification 200x) of the cleaned samples after the experiments in the 50:50 mixture: Alloy 800HT etched with Beraha-II: (a) 480 °C; (b) 680 °C // P9 steel etched with Beraha-I: (c) 480 °C; (d) 680 °C

5.4 Thermodynamic considerations

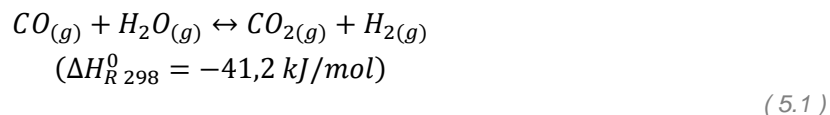
5.4.1 Gas atmosphere with HCl

By interpretation of the different EDX mappings it is possible to give a rough explanation for the main corrosion process in the mixed gas atmosphere with HCl and H₂S.

HCl is able to diffuse through the original chromium oxide layer. At the metal-oxide-interface, where the partial pressure of the oxygen is low enough, it can react with the alloying components and form the corresponding metal chlorides. According to their Gibbs free energy of formation CrCl₂ is formed more likely than FeCl₂. [1] The noble nickel does not react with HCl, because the Gibbs free energy of formation of NiCl₂ is too high. However, if nickel gets in contact with H₂S in the testing gas, the possibility of sulfidation increases with decreasing temperature.

Depending on the temperature, FeCl₂ evaporates constantly due to its high vapour pressure. The now gaseous iron chloride diffuses outwards and can be converted into sulfides, oxides or is carried away with the passing gas stream. Due to the lack of molecular oxygen in the atmosphere the oxygen partial pressure is very low. Therefore the formation of iron oxide during the experiment is rather unlikely. Additionally, oxygen has a much higher affinity to chromium than to iron. At the colder part of the silica glass tube the evacuated FeCl₂ then resublimates. This release of FeCl₂ is the main reason for the mass loss of the specimen during the experiment. Due to the high temperature-dependence of the vapour pressure of FeCl₂, the amount of re-crystallized iron chloride in the silica glass tube decreases with decreasing temperature, and therefore the amount of unmodified FeCl₂ in the corrosion layer increases at lower temperatures. The chloride layer is located beneath the sulfide layers, which explains the reactions of iron and nickel. For understanding the reactions of chromium further consideration have to be done: CrCl₂ has a lower vapour pressure compared to FeCl₂. Nevertheless, its vapour pressure is high enough so that CrCl₂ can diffuse outwards to the surface of the sample with the surrounding gas phase. As soon as it reaches an adequate partial pressure it converts into a chromium sulfide or chromium oxide. Under these conditions chromium oxide is the thermodynamically stable phase, but this does not agree with the mappings of the samples that revealed chromium sulfides as the main phases. This behaviour could be explained with reaction kinetics. To convert to stable Cr₂O₃, CrCl₂ requires further oxygen. Because of the (calculated) oxygen partial pressure of $p_{O_2} = 10^{-25}$ bar, no free O₂ is available in the present gas phase. Although there is some CO₂ present as a possible oxygen source in the atmosphere, this molecule will not react directly with CrCl₂ because of its stability at the given temperatures. Therefore, oxygen must be provided by another, more reactive source.

This could be H₂O produced by the water-gas-shift reaction:



The water-gas-shift reaction is normally used for the H₂ production, which is needed to produce ammonia.[40] It is a moderately exothermic reaction, which means energy will be released during the conversion of the educts into the products. According to the Le Chatelier's principle the equilibrium of this reaction will be shifted towards the reactants, if energy is added.[41] The higher the temperature the more H₂O will be produced. This leads to the possible conclusion that the formation of Cr₂O₃ depends on the slow reaction of CO₂ with H₂ in the gas atmosphere, according to the water-gas-shift reaction. It must be mentioned, that this proposed oxygen source is an assumption only. To verify it, additional experiments are necessary.

Besides CO₂ the testing gas also contains H₂S. Due to the possibility of CrCl₂ to react directly with H₂S without any intermediate reaction, chromium sulfides will grow much faster than the oxides. Moreover, the diffusion coefficients of corresponding sulfides and oxides are different. Chromium sulfide has more defects and therefore a better permeability for the ions, whereas diffusion through the oxide layer is slower. Furthermore, only 200 ppm H₂S are present in the test gas composition. Therefore the reaction of H₂S will only occur in the outer area of the corrosion layer and it is unlikely that it is transported to the base material. The low H₂S concentration in the test gas and the better permeability leads to the formation of the sulfide layer with large sulfide crystals on top of the porous oxide scale. Under the sulfide scale the oxygen partial pressure is then sufficient to form the Cr₂O₃. The constant formation of sulfides and oxides out of the corresponding chlorides releases HCl, which can re-enter the scale and again form chlorides. This process is an auto-catalysed reaction.

The corrosion attack due to the presence of HCl occurs along the grain boundaries. The corrodent can diffuse more easily into the material and react with the single components, because the boundary diffusion is faster than the bulk diffusion.

The main principle of this corrosion process occurs at all three temperatures. Nevertheless, there are some differences due to the strong temperature dependence of the high-temperature corrosion and due to the principle of supply and demand, which plays an important role, especially in case of P9 steel.

Therefore, the corrosion process will be discussed separately for each temperature.

5.4.1.1 480 °C

The vapour pressure of CrCl₂ at 480 °C is about 10⁻⁹ bar [1], which is enough to transport CrCl₂ via the gas phase outwards. As soon as the oxygen or sulfur partial pressures are high enough, CrCl₂ will be converted into either chromium sulfide or chromium oxide.

In case of iron, FeCl_2 will be formed. Its partial pressure at 480 °C is between 10^{-4} and 10^{-5} bar and therefore higher than the partial pressure of CrCl_2 , leading to an accelerated evaporation. Due to the lower chromium concentration of P9 steel compared to alloy 800HT, the amount of formed FeCl_2 on the P9 steel will be much higher. FeCl_2 diffuse outwards and partly gets converted into iron sulfide. Because of the very low oxygen partial pressure and the higher affinity of oxygen to chromium, the formation of iron oxide is very unlikely. In addition, less reactive oxygen is available because of the water-gas-shift-reaction, as discussed above. The main part of the FeCl_2 stays unmodified in the corrosion layer, due to the low temperature.

In case of alloy 800HT nickel is present as an alloying element. It has, at the lowest testing temperature, the highest affinity to sulfur. This led to the highest mass loss for alloy 800HT after 10 days, compared to the other temperatures of 580 °C and 680 °C. Nickel sulfides diffuse through the whole corrosion layer and formed the outer sulfide scale. Nevertheless, nickel is the less reactive component compared to iron and chromium and therefore enriches in the base material. A repeated spalling of the outermost layer led to the formation of a multi-layered corrosion scale. Each layer consists of sulfides and a mixture of chlorides and oxides beneath it.

5.4.1.2 580 °C

At 580 °C the vapour pressure of CrCl_2 is about 10^{-6} bar.[1] The now formed CrCl_2 evaporates more easily compared to 480 °C and gets transported via the gas phase towards the passing gas flow. On its way, it will be converted into an oxide or sulfide as soon as it reaches an area with adequate partial pressures. Due to the higher chromium content in alloy 800HT the chromium depletion of the base material leads to a concentration gradient within the metal. To compensate the concentration gradient, chromium diffuses outwards from the inner part of the metal. Then hydrogen chloride is supplied with new chromium to form CrCl_2 . This process will continue until the diffusion length of the chromium has reached a limiting value. This value is temperature-dependent and will increase with increasing temperature. The so produced chromium depletion can be seen in the EDX mapping of alloy 800HT (Figure 5.23).

Only very few CrCl_2 is converted into Cr_2O_3 , which indicates a negligible water-gas-shift reaction and therefore not many H_2O molecules in the atmosphere to react with the CrCl_2 .

Instead CrCl_2 converts with H_2S into chromium sulfide. The existing Cr_2O_3 is located under the sulfide scale because of the already mentioned different permeability of sulfides and oxides.

Due to the high amount of HCl in the gas atmosphere, not all of it will be consumed by chromium. Therefore, alongside those reactions with chromium, HCl also reacts with iron.

The formed FeCl_2 evaporates constantly due to its higher vapour pressure of about 10^{-3} bar at 580 °C. According to the theory of the quasi-stability diagrams with a critical FeCl_2 partial pressure of 10^{-4} bar, the mass loss due to vaporisation of metal chlorides has reached a significant value at the temperature of 580 °C. The evaporated FeCl_2 either gets carried away with the gas flow or converts into a sulfide. Again, the formation of iron oxide is very unlikely because of the low oxygen partial pressure and the higher affinity to chromium than to iron. The mass loss is mainly caused by vaporisation of FeCl_2 and is higher in P9 steel because of the higher iron content compared to alloy 800HT.

Nickel in the base material of alloy 800HT is inert to HCl attack in the mixed gas atmosphere. Only H_2S can lead to the formation of small amounts of nickel sulfide in the corrosion layer. Apart from that nickel will remain in the base material.

5.4.1.3 680 °C

At a temperature of 680 °C the same mechanism of chromium depletion in comparison with 580 °C is responsible in alloy 800HT. Due to the higher temperature the diffusion and therefore the chromium depletion reaches deeper into the metal. As a consequence a higher amount of CrCl_2 is produced that can then be converted into oxides or sulfides.

The higher temperature additionally leads to a higher H_2O content in the atmosphere and thus to more reactive oxygen. Therefore a more constant Cr_2O_3 layer is formed than at 580 °C. In addition, the diffusion of reactive oxygen reaches deeper into the base material. Beneath the constant Cr_2O_3 layer more Cr_2O_3 formed in the material where the oxygen partial pressure is high enough.

In case of iron a more severe material depletion occurred at 680 °C compared to the lower temperatures due to the accelerated formation and evaporation of iron(II) chloride. The vapour pressure of FeCl_2 at 680 °C is now about 10^{-2} bar. Most of the formed FeCl_2 gets carried away with the gas flow and only small amounts of FeCl_2 get converted into sulfides.

The P9 steel shows, due to its higher iron content, its less chromium content of only 9wt.% and the insignificant nickel content, a more severe mass loss at a temperature of 680 °C compared to alloy 800HT. Gaseous FeCl_2 can easily diffuse through the porous Cr_2O_3 scale on top of the corrosion layer. This fast formation and evaporation of iron(II) chloride is the main reason for the considerable mass loss of P9 steel at 680 °C. Because of the temporary high amount of FeCl_2 in the corrosion scale and the following boundary layer of the P9 steel, a certain amount of FeCl_2 is converted into iron sulfides because of the presence of reactive H_2S and into iron oxide because of the comparable high amount of H_2O in the atmosphere.

Nickel again remains in the base material of alloy 800HT and nearly does not react with HCl. It decreases the sulfidation due to the high temperature as well, which can be seen in the mapping where no nickel sulfide was detected in the corrosion layer.

5.4.2 Gas atmosphere without HCl

The corrosion attack now does not appear along the grain boundaries, but occurs constant, along the whole surface. The determining factor for the reaction rate is the phase boundary reaction in which the sulfur transfer from H_2S takes place. The two materials showed severe differences in their behaviour in the atmosphere without HCl.

Alloy 800HT:

480 °C: At this temperature nickel has the highest affinity to sulfur compared to the other temperatures. Additionally, iron reacts with the sulfur in the atmosphere. This leads to the formation of a mixed iron-nickel sulfide layer. A few iron sulfides also get converted into iron oxides and form an oxide layer beneath the sulfides. The chromium remaining in the base material partly converts to Cr_2O_3 . The oxide layer acts as a diffusion barrier, because of the already mentioned worse permeability compared to the sulfides. This is probably the main reason for the low mass loss of alloy 800HT at this temperature.

680 °C: At 680 °C the affinity of sulfur to chromium increased, which led to the formation of a chromium sulfide layer. The chromium depletion due to sulfide formation results in a concentration gradient within the material. Therefore chromium diffuses outward to compensate this gradient and is now again reachable for sulfur. Due to the higher temperature a faster diffusion rate occurs, which follows a high available amount of chromium. This led to a denser sulfide layer which then acts as a diffusion barrier. Consequently, the transfer of iron to sulfur is inhibited. The high diffusion rate of chromium is thus the main reason for the higher mass loss of the alloy 800HT at 680 °C compared to 480 °C. In addition, a small Cr_2O_3 scale is partly located under the sulfide layer. This acts as diffusion barrier as well.

P9 steel:

480 °C: Sulfur has a higher affinity to iron and nearly does not react with chromium. A part of the formed iron sulfides diffuse outwards via the gas phase and forms large iron sulfide crystals on top of the layer. This leads to iron depletion in the material. Within this area of iron depletion, iron and chromium sulfides are present. At a temperature of 480 °C the mass loss in the sulfidising atmosphere is much higher compared to the environment with additional HCl. This can be explained with the phase boundary reaction. The important factors are the transfer of sulfur from H_2S and the diffusion from iron to sulfur and vice versa. HCl in the mixed gas atmosphere inhibits the sulfur transfer and therefore decreases the sulfidation rate, whereas without HCl sulfur easily can be transferred from H_2S causing a

higher mass loss. The comparatively low temperature prevents formation of oxygen in the gas atmosphere and therefore nearly no oxides are formed.

680 °C: Compared to alloy 800HT nearly no chromium occurs in the sulfide layer at this temperature. This is related to the very low chromium content of only 9wt.%. Therefore sulfur diffuses into the material and reacts more likely with iron than with chromium. Most of the iron sulfides are transported outward and form large iron sulfide crystals on top of the material. Only few sulfides remain in the base material and subsequently form a mixture of iron and chromium sulfides. Due to the higher temperature more H₂O is present as an oxygen source in the atmosphere. Therefore the sulfides in the outermost area are converted with higher rates into iron oxides and form a border around the sulfides. Chromium, remaining in the base material, converts besides sulfides to Cr₂O₃.

5.5 Summary of the proposed corrosion mechanism

Figure 5.48 schematizes the proposed corrosion mechanism in the gas atmosphere with HCl.

Firstly, HCl diffuses through the naturally built Cr_2O_3 scale. It attacks the material along the grain boundaries. HCl then reacts with chromium and iron to form metal chlorides. Due to the values of the Gibbs free energy of formation, CrCl_2 will be formed prior to FeCl_2 . The more noble nickel metal does not react with HCl; nevertheless, the possibility of sulfidation increases with decreasing temperature. The corresponding metal chlorides then evaporate, depending on their vapour pressures. Gaseous FeCl_2 diffuses outwards and either is carried away with the passing gas flow, stays in the corrosion layer or gets converted with H_2S in the atmosphere into sulfides. CrCl_2 is not carried away and only reacts with the components in the testing gas or remains in the corrosion layer. During this process HCl gets released, which then can re-enter the scale to form other metal chlorides. This leads to an auto catalysed process. The formed metal sulfides grow on top of the porous oxide scale. Beneath the corrosion layer a porous structure with metal chlorides is left. FeCl_2 , which gets carried away with the gas flow, is responsible for the mass loss of the samples during the corrosion experiment.

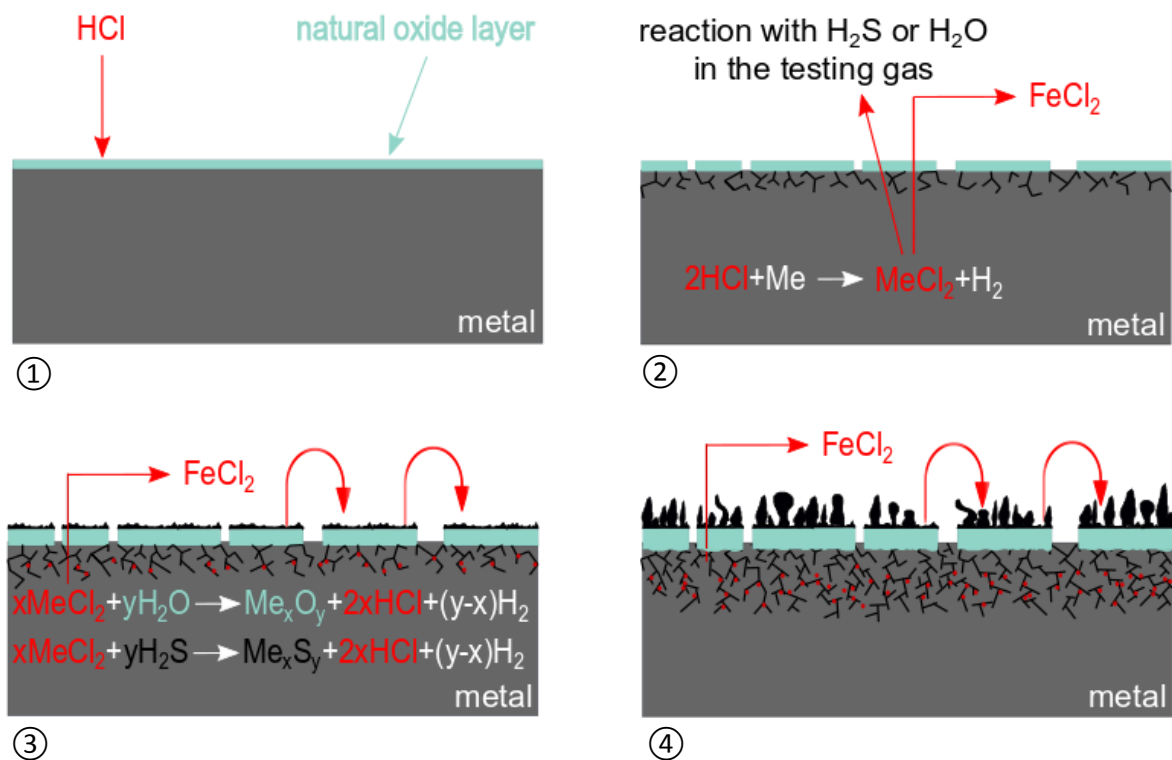


Figure 5.48 Schematic representation of the proposed corrosion mechanism in the mixed gas atmosphere: ① Initiation; ② Attack along grain boundaries and formation of metal chlorides ($\text{Me}=\text{Cr}, \text{Fe}$); ③ Reaction with H_2S and H_2O in the testing gas, formation of oxides and sulfides under release of HCl, re-entering of HCl; ④ Formation of large sulfide crystals on top of porous oxide layer with porous structure beneath it

6 Conclusions

Two materials, alloy 800HT and P9 steel, were tested at 480 °C, 580 °C and 680 °C, in gas atmospheres that mimic the thermal cracking process of anthropogenic recourses. Based on the results of the experiments the following statements can be drawn:

Alloy 800HT and P9 steel show the same main principle corrosion mechanism, in which the formation and evaporation of iron chloride is the main reason for the mass loss of the samples during the corrosion experiment. The high amount of iron in the P9 steel led to a significant mass loss in the HCl-containing gas atmosphere at 680 °C. Alloy 800HT showed very good resistance against the HCl attack at all three temperatures.

The chromium content has only a minor influence on the corrosion resistance, because HCl favours the reaction with chromium and acts as a shuttle which transports chromium out of the material into the corrosion layer, where it can react with the other components of the test gas atmosphere (oxygen, sulfur). HCl also prevents the material to form a protective chromium oxide layer.

Addition of nickel as an alloying element increases the resistance against the chlorine-induced high-temperature corrosion. The sulfidation increases with decreasing temperature, because of the higher affinity of nickel to sulfur at low temperatures in the mixed gas atmosphere.

To sum up, P9 steel should neither be used as a reactor material for the thermal cracking process of anthropogenic recourses nor in applications with mixed gas atmospheres at temperatures above 580 °C occurs. Alloy 800HT with a high nickel content shows a much better resistance at high temperatures and therefore would present a possible reactor material.

References

1. Zahs, A., M. Spiegel, and H.J. Grabke, *Chloridation and oxidation of iron, chromium, nickel and their alloys in chloridizing and oxidizing atmospheres at 400–700°C*. Corrosion Science, 2000. **42**(6): p. 1093-1122.
2. Pan, T., F. Gesmundo, and Y. Niu, *Corrosion behavior of three iron-based model alloys in reducing atmospheres containing HCl and H₂S at 600 C*. Corrosion science, 2007. **49**(3): p. 1362-1377.
3. Sorell, G., *The role of chlorine in high temperature corrosion in waste-to-energy plants*. Materials at high temperatures, 1997. **14**(3): p. 207-220.
4. Zahs, A., M. Spiegel, and H. Grabke, *The influence of alloying elements on the chlorine-induced high temperature corrosion of Fe-Cr alloys in oxidizing atmospheres*. Materials and Corrosion, 1999. **50**(10): p. 561-578.
5. Yu, J., et al., *Thermal degradation of PVC: A review*. Waste Management, 2016. **48**(Supplement C): p. 300-314.
6. Grabke, H.J., M. Spiegel, and A. Zahs, *Role of Alloying Elements and Carbides in the Chlorine-Induced Corrosion of Steels and Alloys*. 2002.
7. Zhang, K., et al., *The Corrosion Behavior of Four Commercial Steels in Reducing Atmospheres Containing HCl At 773–873 K*. Oxidation of Metals, 2004. **62**(5): p. 323-340.
8. Zhou, H., et al., *An overview of characteristics of municipal solid waste fuel in China: Physical, chemical composition and heating value*. Renewable and Sustainable Energy Reviews, 2014. **36**(Supplement C): p. 107-122.
9. Watanabe, N., et al., *Combustible and incombustible speciation of Cl and S in various components of municipal solid waste*. Waste Management, 2004. **24**(6): p. 623-632.
10. Haanappel, V., T. Fransen, and P.J. Gellings, *Chlorine-Induced High Temperature Corrosion: I. Metals and Alloys-A Review*. High Temperature Materials and Processes, 1992. **10**(2): p. 67-90.
11. Handbook, M., *volume 13 Corrosion*. ASM International, 1987. **584**.
12. Kunze, E., *Korrosion und Korrosionsschutz: Bnde 1 bis 6*. 2001: Wiley.
13. Lange, J., *Einführung in die physikalische Chemie : Thermodynamik Kinetik*. 1942, Wien: Wien : Springer.
14. Bedworth, R. and N. Pilling, *The oxidation of metals at high temperatures*. J Inst Met, 1923. **29**(3): p. 529-582.
15. Young, J., *Chapter 1 The Nature of High Temperature Oxidation, in Corrosion Series*, Y. David John, Editor. 2008, Elsevier Science. p. 1-27.
16. DIN, E., *8044: 1999-11 Korrosion von Metallen und Legierungen; Grundbegriffe und Definitionen (ISO 8044: 1999); Dreisprachige Fassung EN ISO 8044: 1999 (Corrosion of metals and alloys; Basic terms and definitions (ISO 8044: 1999); Trilingual version EN ISO 8044: 1999)*. Corrosion of metals and alloys—Basic terms and definitions (ISO 8044: 1999).
17. *Corrosion, in Materials for Engineers*, W.F. Hosford, Editor. 2008, Cambridge University Press: Cambridge. p. 224-230.
18. Revie, R.W., *Corrosion and corrosion control*. 2008: John Wiley & Sons.

References

19. Böllinghaus, T., et al., *Korrosion und Korrosionsschutz*, in *Dubbel: Taschenbuch für den Maschinenbau*, K.-H. Grote and J. Feldhusen, Editors. 2011, Springer Berlin Heidelberg: Berlin, Heidelberg. p. E94-E111.
20. Young, D.J., *Preface*, in *Corrosion Series*, Y. David John, Editor. 2008, Elsevier Science. p. ix-xi.
21. Nielsen, H.P., et al., *The implications of chlorine-associated corrosion on the operation of biomass-fired boilers*. Progress in Energy and Combustion Science, 2000. **26**(3): p. 283-298.
22. Asteman, H. and M. Spiegel, *Investigation of the HCl (g) attack on pre-oxidized pure Fe, Cr, Ni and commercial 304 steel at 400 C*. Corrosion Science, 2007. **49**(9): p. 3626-3637.
23. Ihara, Y., et al., *The corrosion behaviour of iron in hydrogen chloride gas and gas mixtures of hydrogen chloride and oxygen at high temperatures*. Corrosion Science, 1981. **21**(12): p. 805-817.
24. Ihara, Y., et al., *The corrosion behaviour of chromium in hydrogen chloride gas and gas mixtures of hydrogen chloride and oxygen at high temperatures*. Corrosion Science, 1983. **23**(2): p. 167-181.
25. Ihara, Y., et al., *The corrosion behaviour of nickel in hydrogen chloride gas and gas mixtures of hydrogen chloride and oxygen at high temperatures*. Corrosion Science, 1982. **22**(10): p. 901-912.
26. Latreche, H., S. Doublet, and M. Schütze, *Development of Corrosion Assessment Diagrams for High Temperature Chlorine Corrosion. Part I: State of the Art and Development of the Basis for a New Extended Approach*. Oxidation of metals, 2009. **72**(1-2): p. 1-30.
27. John, R., *1.11 - Sulfidation and Mixed Gas Corrosion of Alloys A2 - Cottis, Bob*, in *Shreir's Corrosion*, M. Graham, et al., Editors. 2010, Elsevier: Oxford. p. 240-271.
28. Young, J., *Corrosion by Sulfur*. Corrosion Series, 2008. **1**: p. 361-396.
29. Mrowec, S., *The problem of sulfur in high-temperature corrosion*. Oxidation of Metals, 1995. **44**(1): p. 177-209.
30. Mrowec, S. and K. Przybylski, *Transport properties of sulfide scales and sulfidation of metals and alloys*. Oxidation of Metals, 1985. **23**(3-4): p. 107-139.
31. Bakker, W., *High temperature corrosion in gasifiers*. Materials Research, 2004. **7**: p. 53-59.
32. Haanappel, V., et al., *Corrosion kinetics of low-and high-alloy steels in chlorine-containing gas atmospheres*. Corrosion, 1992. **48**(10): p. 812-821.
33. Kässens, M., R. Reimer, and R. Wegerhoff, *Mikroskopische Verfahren*, in *Romeis - Mikroskopische Technik*, M. Mulisch and U. Welsch, Editors. 2015, Springer Berlin Heidelberg: Berlin, Heidelberg. p. 1-42.
34. Crankovic, G.M., *ASM Handbook, Volume 10:: Materials Characterization*. 1986: ASM International.
35. *Röntgenbeugung*, in *Kristallstrukturbestimmung*. 2007, Vieweg+Teubner: Wiesbaden. p. 25-42.
36. A. Schmid, G.M., S. Strobl, R. Haubner, S. Hönig, *Corrosion of various Fe and Ni based alloys in HCl, H₂S containing environments, with low oxygen partial pressure, at 680 °C*. Conference Proceedings EUROCORR 2017, 2017. **Paper-Nr. 79016, 10 S.**
37. Schwalm, C. and M. Schütze, *The corrosion behavior of several heat resistant materials in air+ 2 vol-% Cl₂ at 300 to 800° C. Part I-Fe-base and Fe-containing alloys*. Materials and Corrosion, 2000. **51**(1): p. 34-49.

References

38. Bender, R. and M. Schütze, *The role of alloying elements in commercial alloys for corrosion resistance in oxidizing-chloridizing atmospheres. Part I: Literature evaluation and thermodynamic calculations on phase stabilities*. *Materials and Corrosion*, 2003. **54**(8): p. 567-586.
39. Brauer, G., *Handbuch der präparativen anorganischen Chemie*. 2. 1962: Enke.
40. Smith, B., et al., *A Review of the Water Gas Shift Reaction Kinetics*. Vol. 8. 2010.
41. Atkins, P.W. and J. De Paula, *Physikalische Chemie*. Weinheim : Wiley-VCH: Weinheim.